Monsoon-driven biogeochemical dynamics in an equatorial shelf sea: time-series observations in the Singapore Strait

Patrick Martin[1,*], Molly A. Moynihan[1,2,†] , Shuang Chen[1,‡], Oon Yee Woo[1], Yongli Zhou[1], Robert S. Nichols[1,¶], Kristy Y.W. Chang[1,§], Ashleen S.Y. Tan[1,#], Ying-Hsuan Chen[3], Haojia Ren[3], Mengli Chen[4]

[1]Asian School of the Environment, Nanyang Technological University, 639798 Singapore

[2]Earth Observatory of Singapore, Interdisciplinary Graduate School, Nanyang Technological University, 639798 Singapore

[3]Department of Geosciences, National Taiwan University, Taipei 106, Taiwan

[4]Tropical Marine Science Institute, National University of Singapore, 119227 Singapore

Corresponding author: pmartin@ntu.edu.sg

[†]Present address: Marine Biological Laboratory, Woods Hole, MA 02543, USA

[‡]Present address: Kenyon Pte Ltd, 509016 Singapore.

[¶]Present address: DHI Water & Environment (S) Pte Ltd, 608526 Singapore

[§]Present address: Singapore Centre for Environmental Life Sciences Engineering, Nanyang Technological University, 637551 Singapore

[#]Present address: Surbana Jurong Pte Ltd, 150168 Singapore

Keywords

Nutrient dynamics; Dissolved organic matter; Coastal biogeochemistry; Tropical peatland rivers; Southeast Asia

Abstract

Coastal tropical waters are experiencing rapid increases in anthropogenic pressures, yet coastal biogeochemical dynamics in the tropics are poorly studied. We present a multi-year biogeochemical time series from the Singapore Strait in Southeast Asia's Sunda Shelf Sea. Despite being highly urbanised and a major shipping port, the strait harbours numerous biologically diverse habitats, and is a valuable system for understanding how tropical marine ecosystems respond to anthropogenic pressures. Our results show strong seasonality driven by the semi-annual reversal of ocean currents: dissolved inorganic nitrogen (DIN) and phosphorus varied from ≤0.05 μmol l^{-1} during the intermonsoons to ≥4 μmol l^{-1} and ≥0.25 μmol l^{-1}, respectively, during the southwest monsoon. $Si(OH)_4$ exceeded DIN year-round. Based on nutrient concentrations, their relationships to salinity and coloured dissolved organic matter, and the isotopic composition of NO_x^-, we infer that terrestrial input from peatlands is the main nutrient source. This input delivered dissolved organic carbon (DOC) and nitrogen, but was notably depleted in dissolved organic phosphorus. In contrast, particulate organic matter showed little seasonality, and the $\delta^{13}C$ of particulate organic carbon (-21.0 ± 1.5‰) is consistent with a primarily autochthonous origin. Diel changes in dissolved O_2 varied seasonally with a pattern that suggests that light availability controls primary productivity more than nutrient concentrations. However, diel changes in pH were greater during the southwest monsoon, when remineralisation of terrestrial DOC lowers the seawater buffer capacity. We conclude that terrestrial input results in mesotrophic conditions, and that the strait might be vulnerable to further eutrophication if nutrient inputs increase during seasons when light availability is high. Moreover, the seasonality of diel pH variation suggests that coral reefs exposed to terrestrial organic matter in the Sunda Shelf may be at significant risk from future ocean acidification.

1. Introduction

Tropical shelf seas are ecologically and economically important, but are under increasing anthropogenic pressure from coastal development, land-use change, resource extraction, and terrestrial inputs (Jennerjahn, 2012). At the same time, our understanding of the biogeochemistry of tropical shelf seas is more limited than for higher-latitude environments, which makes it harder to predict how anthropogenic pressures will affect tropical seas (Lønborg et al., 2021b; Vieillard et al., 2020).

Tropical coastal waters are usually nutrient-poor because shelf seas exchange large volumes of water with adjacent nutrient-poor open oceans (Brunskill, 2010). However, tropical coastal waters also receive more than half of the global river discharge and nutrient input (Jennerjahn, 2012; Mayorga et al., 2010). Nutrient concentrations and ratios delivered by tropical rivers can be different from temperate regions: for example, tropical rivers typically have higher dissolved silicon concentrations (Jennerjahn et al., 2006). While consistently high temperature and sunlight in the tropics allow for fast rates of uptake and biogeochemical transformation of nutrients in shelf waters, high input of sediments and dissolved organic matter in the tropics can also attenuate sunlight and potentially slow the rates of nutrient utilisation (Nittrouer et al., 1995). As anthropogenic nutrient input is projected to increase substantially within the next decades, particularly in tropical Asia (Sinha et al., 2019), it is pressing to better understand the biogeochemistry of tropical coastal waters.

Southeast Asia's Sunda Shelf Sea is one of the largest and most biodiverse shelf seas globally; however, it also has dense human populations along the coast, placing a high degree of pressure on its marine habitats (Jennerjahn, 2012; Veron et al., 2009). This is especially the case in urbanised marine ecosystems that experience high anthropogenic stress (Heery et al., 2018; Todd et al., 2019). The Sunda Shelf Sea receives a large amount of precipitation and river input that deliver freshwater (Lee et al., 2019), terrestrial carbon (Baum et al., 2007;

Huang et al., 2017; Zhou et al., 2019), and dissolved nutrients (Jennerjahn et al., 2004; Jiang et al., 2019). The climate is driven by the Asian monsoon system, which results in seasonally varying patterns of precipitation across the region and causes a semi-annual reversal in physical ocean circulation across the shelf (Lee et al., 2019; Susanto et al., 2016). While these environmental conditions might be expected to result in dynamic coastal biogeochemistry, the biogeochemistry of Southeast Asia's coastal seas has received comparatively little research attention to date (Partelow et al., 2018). Across the open waters of the Sunda Shelf, chlorophyll-*a* concentrations are typically ≤0.2 μg l^{-1} (Kartadikaria et al., 2015; Ke et al., 2014), indicative of oligotrophic waters. Closer to shore and within estuaries, significant levels of eutrophication due to nutrient input have been reported (Chai et al., 2021; Damar et al., 2019; Lim et al., 2021; Lim et al., 2018; Tomascik et al., 1994). However, very few studies have collected multi-year biogeochemical time series in Southeast Asia, and where such time series do exist (Lim et al., 2018), often only a limited number of parameters are available. This limits our understanding of the drivers of coastal biogeochemistry in Southeast Asia.

Here, we present time-series data collected over multiple years in the Singapore Strait, an urbanised coastal area in the central Sunda Shelf, to examine the dynamics and drivers of nutrient biogeochemistry, and their potential impacts on planktonic productivity. This study complements our previous analyses of seawater carbonate system and bio-optical variability in the Singapore Strait, which revealed a strong seasonal input of terrigenous dissolved organic matter from regional peatlands (Martin et al., 2021; Zhou et al., 2021).

2. Materials and Methods

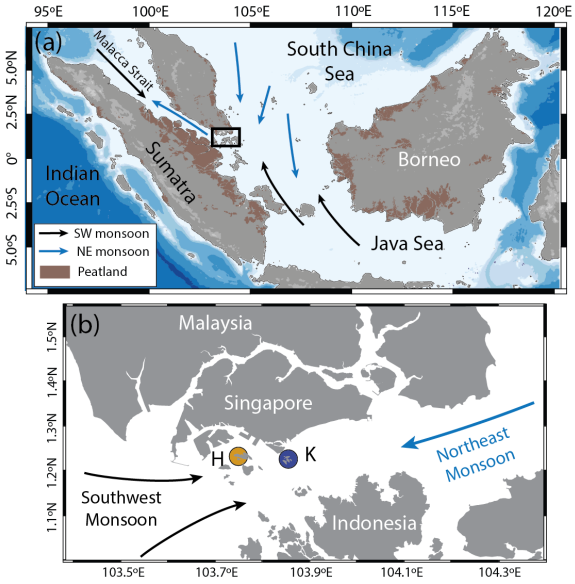

Fig. 1 Map of the study region, modified from Martin et al. (2021), indicating the seasonal current reversal between southwest (SW) and northeast (NE) monsoons (arrows). Yellow marker in (a) indicates the Singapore Strait. The two sampling sites, Hantu ("H") and Kusu ("K") are indicated in (b) by the two crossed yellow circles.

2.1 Site description and study design

The Singapore Strait is situated in the central part of the Sunda Shelf Sea at 1.2°N 103.8°E (Fig. 1) and is subject to two monsoon seasons (Mayer et al.; Susanto et al.; van Maren & Gerritson). During the northeast (NE) monsoon (mid-November to March), the prevailing mean circulation carries water from the open South China Sea across the Sunda Shelf, west- and northwards through the Singapore Strait and the Malacca Strait, and southwards into the Java Sea. During the southwest (SW) monsoon (mid-May to mid-September), the circulation reverses and water flows northwards from the Java Sea towards the South China Sea, while the flow in the Malacca Strait ceases or flows weakly southwards. Flow through the Singapore Strait is then eastwards and out towards the open South China Sea. The annual mean flow follows the direction of the NE monsoon, forming the South China Sea limb of the

Indonesian Throughflow. During the two intermonsoon periods (April to mid-May and mid-September to mid-November) the mean residual flow through the Singapore Strait stagnates. Singapore experiences rainfall year-round, but rainfall is highest during the early NE monsoon (mid-November to January) and is lowest during the late NE monsoon and early intermonsoon (February and March). Because the seawater chemistry changes considerably from early to late NE monsoon, but the late NE monsoon and first intermonsoon are very similar, for the purposes of our analysis we classify March as part of intermonsoon 1, consistent with our previous work (Martin et al., 2021; Zhou et al., 2021). We thus define the seasons as: NE monsoon = 15 Nov to end Feb; intermonsoon 1 = 01 Mar to 15 May; SW monsoon = 15 May to 15 Sept; intermonsoon 2 = 15 Sept to 15 Nov.

Because of the reversing ocean circulation, the Singapore Strait is influenced by considerable river input from Sumatra and the western Malay Peninsula during the SW monsoon, with a notable seasonal decrease in salinity (Tanzil et al., 2019; Zhou et al., 2021) and input of terrestrial dissolved organic matter (DOM) from regional peatlands (Martin et al., 2021; Zhou et al., 2021). During the early NE monsoon, there is freshwater input from local rainfall and river flow, with a shorter period of reduced salinity and a small input of terrestrial DOM (Martin et al., 2021; Zhou et al., 2021).

Here, we present time-series data collected by regular *in-situ* water sampling at two sites in the Singapore Strait, Kusu Island (1.226°N 103.860°E) and Hantu Island (1.227°N 103.746°E) (Fig. 1). Both sites are small islands with narrow fringing reefs, with diverse communities of hard corals down to approximately 6–8 m depth (Guest et al., 2016; Huang et al., 2009). Below this depth, the seafloor consists largely of soft sediment and slopes down to 15–20 m. Sampling started in mid-2015 on an opportunistic basis for inorganic nutrients, and was carried out at monthly to bi-weekly frequency from mid-2017 for an increasing number of parameters.

145 *2.2 Sensor installation*

146 In mid-2015, a Seabird SeaCat 19plusV2 conductivity-temperature-depth sensor (CTD) and a
147 SeaFET pH sensor (previously Satlantic, now Seabird) were installed at approximately 5 m
148 depth on the reef slope of Kusu Island, using iron stakes such that the sensors were
149 approximately half a metre above the seafloor. In mid-2017, a PME miniDOT dissolved
150 oxygen sensor was added at the same depth. The SeaFET and the miniDOT were both
151 equipped with copper biofouling guards; the SeaCat had no antifouling protection but was
152 operated with the pump running during sampling to prevent sediment accumulation in the
153 conductivity cell. All sensors were installed horizontally (except the miniDOT, which
154 initially faced upwards but was then installed horizontally to prevent sediment accumulation
155 between the biofouling guard and the sensor membrane) and measured every 10 min. Sensors
156 were recovered for data download and cleaning every 1–4 months. Gaps in the sensor records
157 occurred as a result of occasional technical problems, the need for maintenance back in the
158 laboratory and factory recalibration, and periods of bad data (see Section 2.5).
159 All salinity data are expressed on the practical salinity scale.
160

161 *2.3 Water sampling*

162 Water samples were collected with a Niskin bottle at 5 m depth, and a CTD profile was
163 measured using a Valeport FastCTD with chlorophyll-*a* fluorometer. Prior to October 2017,
164 samples were only collected for dissolved inorganic nutrient analysis, by syringe-filtering
165 (0.2 µm Acrodisc polyethersulfone [PES] filters, 25 mm diameter) water into acid-washed,
166 15 ml polypropylene centrifuge tubes. From October 2017, a larger number of parameters
167 was measured, and sample water was filtered directly from the Niskin bottle with a peristaltic
168 pump and an in-line polycarbonate filter housing (Pall, product 1119) using 0.2 µm PES
169 membranes (47 mm diameter, Supor, Millipore). The filter, tubing, and filter housing were

rinsed with 300 ml ultrapure water (18.2 MΩ cm^{-1}, hereafter Elga water) and about 100 ml sample water immediately before samples were collected.

Water for $\delta^{13}C$ of dissolved inorganic carbon ($\delta^{13}C$-DIC, 1 ml) was filtered into a syringe without allowing air contact and injected into a He-flushed 12 ml Exetainer (Labco, UK) with butyl rubber septum containing 1 ml of 80% H_3PO_4. Water for DIC concentration was filled to overflowing into 12 ml Exetainers and capped with minimal headspace with a butyl rubber septum. Water for total alkalinity (TA) was filled into 125 ml acid-washed high-density polyethylene (HDPE) bottles. Water for dissolved organic carbon (DOC) and coloured dissolved organic matter (CDOM) was filled into pre-ashed (450°C, 4 hours) 40 ml amber borosilicate vials with PTFE-lined septa. Water for $\delta^{13}C$ of DOC ($\delta^{13}C$-DOC) was filled into 50 ml acid-washed polypropylene centrifuge tubes. Water for dissolved organic and inorganic nutrients was filled into acid-washed 15 ml polypropylene centrifuge tubes. Water for nitrate isotopes ($\delta^{15}N$- and $\delta^{18}O$-NO_x^-) was filled into acid-washed 125 ml HDPE bottles. Samples for dissolved nutrients were immediately frozen in cryogenic dry shippers in the field. All other samples were stored at ambient temperature in the dark until return to the lab (within 2–5 hours). All samples were then stored at +4°C except for dissolved nutrients, $\delta^{15}N$- and $\delta^{18}O$-NO_x^- (-20°C), $\delta^{13}C$-DOC (-20°C), and $\delta^{13}C$-DIC (room temperature). Samples for DOC concentration were acidified on the day of collection with 100 µl 50% H_2SO_4 per 30 ml sample.

In addition, unfiltered water was collected in the field into 1 l acid-washed HDPE bottles to measure particulate organic carbon (POC) and particulate nitrogen (PN), particulate phosphorus (PP), $\delta^{13}C$ of POC ($\delta^{13}C$-POC), $\delta^{15}N$ of PN ($\delta^{15}N$-PN), and chlorophyll-*a*. These samples were stored at ambient temperature in the dark until return to the laboratory, and then vacuum-filtered (0.5–1.5 l, depending on date and parameter) onto 25 mm Whatman GF/F filters (nominal pore size 0.7 µm). Except for chlorophyll-*a*, all GF/F filters were pre-

ashed (450°C 4 hours), and samples were briefly rinsed with Elga water upon filtration. All samples were then wrapped in aluminium foil and frozen at -20°C, except chlorophyll samples, which were flash-frozen in liquid nitrogen and stored at -80°C.

2.4 Analyses

2.4.1 Dissolved nutrients and organic matter

Dissolved inorganic nutrients, i.e. nitrate (NO_3^-), nitrite (NO_2^-), ammonia (NH_4^+), phosphate (PO_4^{3-}), and silicate ($Si(OH)_4$), were analysed on a SEAL AA3 segmented-flow autoanalyser. The methods for $NO_3^- + NO_2^-$, NO_2^-, PO_4^{3-}, and $Si(OH)_4$ followed the colorimetric techniques outlined in Hansen and Koroleff (1999) according to SEAL methods G172, G173, G297, and G177. NH_4^+ was analysed fluorometrically after reaction with o-phthaldialdehyde according to SEAL method G327, based on Kérouel and Aminot (1997). Detection limits were 0.05 µmol l^{-1} ($NO_3^- + NO_2^-$), 0.01 µmol l^{-1} (NO_2^-), 0.016 µmol l^{-1} (PO_4^{3-}), 0.1 µmol l^{-1} ($Si(OH)_4$), and 0.25 µmol l^{-1} (NH_4^+).

Dissolved organic nitrogen and phosphorus (DON and DOP) were analysed as for inorganic NO_3^- and PO_4^{3-} following wet oxidation. 4.5 ml of sample water were mixed in glass centrifuge tubes with 0.5 ml of a solution consisting of 6 g $K_2S_2O_8$ with 3 g $B(OH)_3$ in 100 ml of 0.42 M NaOH, tightly capped and autoclaved at 120°C for 30 min, and diluted 1:1 with artificial seawater prior to analysis. For DOP analysis, we introduced an additional ascorbic acid solution with the first reagent line (instead of just surfactant as for inorganic PO_4^{3-} analysis), such that the solution stream on the AA3 had a concentration of 40 mmol l^{-1} ascorbic acid before the colour reagents were introduced. This reduces interference from chlorine species generated during wet oxidation (Ma et al., 2017). Oxidation efficiency was monitored with ethylenediamine tetraacetic acid (DON) and glucose-6-phosphate (DOP), and was always ≥92%.

Dissolved organic carbon (DOC) was analysed on a Shimadzu TOC-L instrument equipped with the manufacturer's high-salt kit, calibrated with potassium hydrogen phthalate standards, and validated using the University of Miami deep-sea certified reference material. Coloured dissolved organic matter (CDOM) was measured on a Thermo Evolution300 dual-beam spectrophotometer against Elga water as the reference using 10-cm pathlength quartz cuvettes. Data were baseline corrected (Green and Blough, 1994), smoothed using a loess function, and converted to Napierian absorption coefficients. We use the CDOM absorption coefficient at 350 nm, a_{350}, as a measure of CDOM concentration.

2.4.2 Particulate C, N, and P

Particulate organic carbon (POC) and particulate nitrogen (PN) were analysed together after acid-fuming the filters overnight in a desiccator with concentrated HCl, then drying them overnight at 40°C, and pelleting the samples in tin foil discs (Sercon, SC1032). They were then analysed at the University of Hong Kong on a Eurovector elemental analyser and Nu Instruments Perspective isotope ratio mass spectrometer (IRMS) calibrated with acetanilide standards. Particulate phosphorus (PP) was measured by submerging filters in 3 ml of oxidative solution (made as for DOP analysis) in tightly-capped glass centrifuge tubes and autoclaving them for 30 min at 120°C. Samples were then diluted between 1:40 and 1:100 with artificial seawater and analysed as for inorganic PO_4^{3-}; the high dilution in this case eliminates the need for additional ascorbic acid. Oxidation efficiency was monitored with glucose-6-phosphate and was always >88%.

2.4.3 Isotope analyses

Stable carbon and nitrogen isotopes of POC and PN (δ^{13}C-POC and δ^{15}N-PN) were measured with a separate set of filters from POC and PN concentration measurements, for which a

larger volume of water was filtered to yield higher instrument signals. These filters were not acid-fumed, because calcifying plankton species are essentially absent from these waters. Samples were otherwise prepared and analysed as for POC/PN analysis, but without using acetanilide concentration standards. Instead, the analysis was calibrated with isotope standards USGS40 and 41a. Analytical precision was assessed with acetanilide standard 1 from University of Indiana, and was ±0.2‰ or better for both $\delta^{13}C$ and $\delta^{15}N$.

$\delta^{15}N$- and $\delta^{18}O$-NO_x^- was analysed on a subset of samples from Kusu in 2019–2020 for which the NO_3^- concentration was sufficiently high. Analysis was performed using an IRMS after converting all NO_x^- into N_2O with the denitrifying bacterium *Pseudomonas chlororaphis* strain ATCC 13985 (Sigman et al., 2001). During the analysis, the standard reference materials IAEA-NO_3^- (-1.8‰ vs. air) and USGS 34 (4.7‰ vs. air) were prepared every 8-10 samples to constrain the performance of the bacterial conversion and the stability of the mass spectrometer. The stability of the mass spectrometer was further monitored by a series of prepared N_2O gas vials at the beginning and the end of each run and every 10 samples. The average standard deviation of the $\delta^{15}N$ measurements on sample replicates was less than ±0.1‰.

$\delta^{13}C$-DIC was analysed partly at the UC Davis Stable Isotope Laboratory and partly at Nanyang Technological University using a Gas Bench connected to a Thermo Delta V IRMS, as described by Zhou et al. (2021). Analytical precision was ±0.1‰ at UC Davis and ±0.2‰ for our in-house analysis.

2.4.4 Chlorophyll-a

Chlorophyll-*a* was measured on a Horiba Fluoromax4 spectrofluorometer at excitation 436 nm and emission 680 nm (both with bandpass of 5 nm) according to Welschmeyer (1994), after extracting the samples in 90% acetone at +4°C overnight in the dark. Samples were

thoroughly mixed and centrifuged at 500 rcf for 10 min prior to analysis. Calibration was performed using spinach chlorophyll-*a* (Sigma-Aldrich, C5753).

2.5 Sensor data quality control and analysis

The Valeport CTD profiles were used to calculate the mean salinity, temperature, and chlorophyll-*a* between 4.5 and 5.5 m depth to accompany our water sample data. The chlorophyll fluorometer malfunctioned and returned values consistently below 0.1 $\mu g\ l^{-1}$ between October 2018 and July 2019 until the fault was repaired; these measurements have been omitted.

All data from the moored sensors were checked manually to remove spikes and periods with suspect data, e.g. when heavy biofouling was noted on the sensor parts. For dates when both SeaCAT and Valeport data were available, the Valeport data were compared to the SeaCAT measurement closest in time; except for two outliers in salinity, the data agreed with root mean squared error (RMSE) of ±0.07 (salinity) and ±0.08°C (Fig. S1).

The SeaFET data were compared to pH calculated from TA and DIC, which were measured during each sampling date starting in August 2018. pH was calculated using the R package *seacarb* (Gattuso et al., 2016) based on the Valeport salinity and temperature and the measured dissolved inorganic nutrient concentrations. We used the dissociation constants from Lueker et al. (2000) for carbonic acid, from Dickson (1990) for HSO_4^-, and from Perez and Fraga (1987) for fluoride; total boron concentration followed Uppström (1974). The SeaFET pH data were first reprocessed based on the salinity record from the SeaCAT, and were then compared to the calculated pH based on TA and DIC measurements. For dates when no SeaCAT data were available, a salinity of 30 was assumed for the SeaFET data processing (note that the salinity correction is too small to impact our results significantly). A direct comparison of our TA+DIC-based calculated pH with the closest matching individual

SeaFET pH measurement for all dates when good-quality SeaFET measurements were available within 3 hours of the water sampling showed that the data clustered around the 1:1 line with root mean squared error of 0.028 pH units across a pH range of 7.85–8.01 (Figure S1).

Lab-based measurements of dissolved oxygen concentration are not available for comparison to the miniDOT. Hence, the data were only examined qualitatively to remove periods where either the diel amplitude increased considerably or we observed a clear decrease in daily average concentration together with a large increase in diel amplitude. These cases were suspected to be caused by biofouling and/or accumulation of excessive amounts of suspended particulate matter on the sensor interface, as the variability decreased again after sensor cleaning.

2.6 Data analysis and previous data use

All data analysis and plotting were carried out in R (R Core Team, 2020). To test for seasonal variation, we used non-parametric Kruskal-Wallis tests with post-hoc Dunn tests. All averages are quoted as mean ± standard deviation unless specified otherwise.

The majority of the data for salinity, temperature, DOC, CDOM, chlorophyll-*a*, δ^{13}C-DOC, δ^{13}C-DIC, and the daily averages of seawater pH were previously used in our analyses of carbonate system variability (Zhou et al., 2021) and bio-optical variability (Martin et al., 2021). The data for dissolved inorganic nitrogen, PO_4^{3-}, and chlorophyll-*a* are also used in an analysis of alkaline phosphatase activity in the Singapore Strait (Nichols et al., submitted manuscript).

3. Results

3.1 Hydrographic variability

Salinity and temperature ranged typically between 29–33 and 28–31°C and showed pronounced seasonal variation, with highest values during the late NE monsoon and intermonsoon 1 seasons (February to early May), and also during intermonsoon 2 (mid-September to mid-November) (Fig. 2). Salinity and temperature decreased during both monsoon seasons, but with distinct patterns: salinity was lowest throughout the SW monsoon (mid-May to mid-September), but only decreased for a shorter period during the early NE monsoon (mid-November to January) and not always by as much as during the SW monsoon. Temperature decreased more strongly during the NE monsoon and less during the SW monsoon. While temperature was essentially identical between both sites, the salinity during the SW monsoon was consistently lower at Hantu than at Kusu by an average of 0.49 ± 0.22. Both sites typically showed little vertical density variation without a clear pycnocline (Fig. S2), confirming that the water column is generally well mixed.

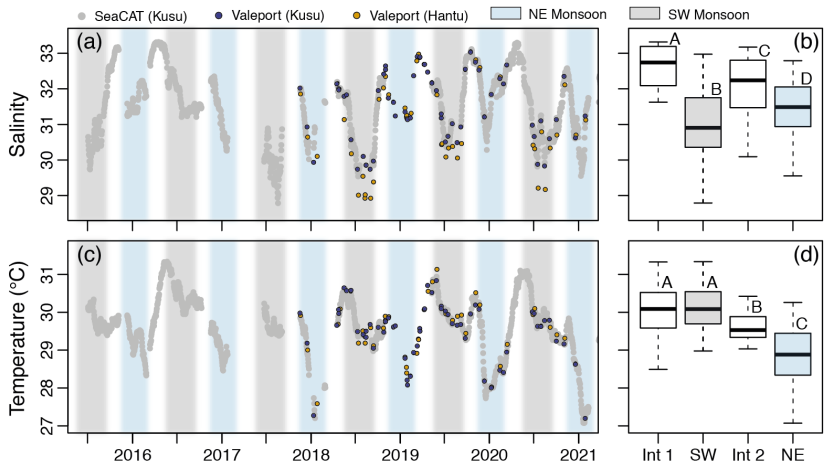

Fig. 2. Time series and seasonal boxplots of (a,b) salinity and (c,d) temperature in the Singapore Strait. Grey shading indicates the southwest (SW) monsoon, blue shading indicates the northeast (NE) monsoon. In the boxplot x-axis, Int 1 = intermonsoon 1; SW = southwest monsoon; Int 2 = intermonsoon 2; NE = northeast monsoon. Data from the Seabird SeaCAT moored CTD (at Kusu) are daily mean values; data from the Valeport FastCTD are from profiling measurements averaged at 5 m. Letters in the boxplots indicate significant differences between seasons (Kruskal-Wallis with post-doc Dunn test, $p<0.05$).

340 *3.2 Dissolved inorganic nutrients*

341 Except for NH_4^+, the dissolved inorganic nutrient concentrations also showed very strong and
342 statistically significant seasonal variation, with elevated concentrations during the SW
343 monsoon, a smaller and shorter increase during the early NE monsoon, and mostly very low
344 concentrations (often close to or below detection limits) during both intermonsoon periods
345 (Fig. 3; Table 1). Concentrations of NO_3^- + NO_2^- reached 4–5 µmol l^{-1} during the SW
346 monsoon, with NO_2^- typically contributing 0.5–1.0 µmol l^{-1} during this time, but NH_4^+ was
347 only sporadically detectable (usually during the NE monsoon), with highest concentrations
348 during 2018 (Fig. 3a-f). PO_4^{3-} showed very similar seasonal patterns to NO_3^- + NO_2^-, with
349 values ranging from below detection to around 0.35 µmol l^{-1} (Fig. 3g,h). $Si(OH)_4$ differed
350 slightly from the other nutrients in never dropping below detection limits, and was >2 µmol l^{-1}
351 in all but seven samples, reaching up to 13.8 µmol l^{-1} (Fig. 3i,j). Moreover, $Si(OH)_4$ showed
352 clearer peaks during the NE monsoon than the other nutrients.

353

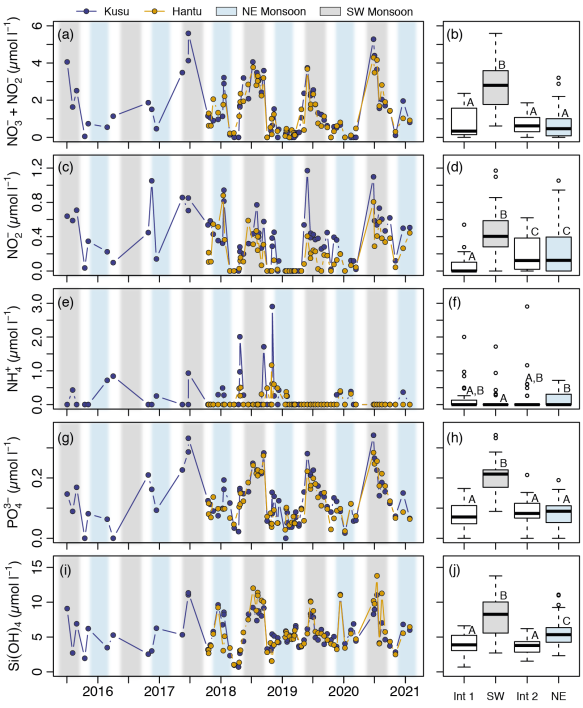

354

355 Fig. 3. Time series and seasonal boxplots of dissolved inorganic nutrient concentrations in the Singapore Strait.
356 Colour shading and boxplot labelling are as in Fig. 2.

Parameter		Intermonsoon 1	SW monsoon	Intermonsoon 2	NE monsoon	χ^2	p
Salinity (daily mean)	Min, Max	31.63, 33.32	28.79, 32.97	30.09, 33.17	29.55, 32.79		
	Mean (SD)	32.63 (0.53)	31.01 (0.85)	32.09 (0.79)	31.44 (0.70)		
	Median	32.74	30.90	32.24	31.49	547	<0.0001
Temperature (daily mean)	Min, Max	28.49, 31.33	28.98, 31.34	29.03, 30.42	27.07, 30.26		
	Mean (SD)	30.06 (0.66)	30.14 (0.52)	29.64 (0.37)	28.81 (0.75)		
	Median	30.09	30.08	29.53	28.88	662	<0.0001
pH (daily mean)	Min, Max	7.942, 7.999	7.821, 7.99	7.859, 8.033	7.865, 8.035		
	Mean (SD)	7.968 (0.013)	7.896 (0.037)	7.937 (0.048)	7.980 (0.034)		
	Median	7.964	7.888	7.937	7.987	440	<0.0001
Dissolved O_2 (daily mean)	Min, Max	155, 193	164, 195	169, 207	155, 198		
	Mean (SD)	181 (9.8)	178 (6.1)	184 (5.8)	180 (11.7)		
	Median	183	179	183	180	43.6	<0.0001
Diel change in pH	Min, Max	0.014, 0.103	0.019, 0.1589	0.017, 0.1444	0.010, 0.162		
	Mean (SD)	0.056 (0.020)	0.068 (0.023)	0.059 (0.022)	0.041 (0.019)		
	Median	0.0563	0.0662	0.0556	0.0366	262	<0.0001
Diel change in dissolved O_2	Min, Max	15.3, 78.3	13.5, 80.5	11.8, 69.5	10.0, 63.4		
	Mean (SD)	39.5 (13.2)	35.3 (13.8)	32.8 (12.6)	28.3 (10.2)		
	Median	40.1	32.2	31.5	27.0	31.1	<0.0001
$NO_3^- + NO_2^-$	Min, Max	<0.05, 2.37	0.613, 5.60	<0.05, 1.86	<0.05, 3.21		
	Mean (SD)	0.803 (0.817)	2.74 (1.16)	0.704 (0.523)	0.733 (0.816)		
	Median	0.332	2.80	0.621	0.467	71.6	<0.0001
NO_2^-	Min, Max	<0.01, 0.538	<0.01, 1.17	<0.01, 0.620	<0.01, 1.05		
	Mean (SD)	0.071 (0.126)	0.451 (0.251)	0.208 (0.201)	0.241 (0.292)		
	Median	<0.01	0.404	0.122	0.125	42.9	<0.0001
NH_4^+	Min, Max	<0.25, 2.01	<0.25, 1.72	<0.25, 2.90	<0.25, 0.719		
	Mean (SD)	0.211 (0.474)	0.075 (0.285)	0.210 (0.575)	0.149 (0.200)		
	Median	<0.25	<0.25	<0.25	<0.25	8.78	0.032
PO_4^{3-}	Min, Max	<0.016, 0.165	0.089, 0.342	<0.016, 0.210	<0.016, 0.193		
	Mean (SD)	0.080 (0.045)	0.206 (0.054)	0.089 (0.041)	0.085 (0.042)		
	Median	0.071	0.213	0.083	0.090	82.3	<0.0001
$Si(OH)_4$	Min, Max	0.688, 6.62	2.71, 13.77	1.54, 6.20	2.32, 11.08		
	Mean (SD)	3.89 (1.69)	7.88 (2.57)	3.70 (1.14)	5.60 (2.09)		
	Median	3.89	8.26	3.79	5.35	61.6	<0.0001
POC	Min, Max	8.74, 19.9	6.78, 29.8	8.33, 22.3	7.84, 22.3		
	Mean (SD)	13.5 (3.48)	11.7 (4.21)	14.0 (3.28)	14.2 (3.81)		
	Median	13.6	11.2	13.6	13.2	11.9	0.008
PN	Min, Max	1.41, 3.63	0.97, 5.35	1.49, 3.32	1.23, 4.19		
	Mean (SD)	2.39 (0.75)	2.08 (0.80)	2.46 (0.51)	2.50 (0.80)		
	Median	2.18	2.06	2.58	2.16	7.89	0.048
PP	Min, Max	0.02, 0.19	0.01, 0.16	0.05, 0.20	0.05, 0.22		
	Mean (SD)	0.08 (0.04)	0.07 (0.03)	0.10 (0.04)	0.11 (0.04)		
	Median	0.08	0.07	0.08	0.11	22.6	<0.0001
δ^{13}C-POC	Min, Max	-24.8, -17.1	-24.2, -18.0	-23.2, -19.3	-22.3, -18.0		
	Mean (SD)	-20.9 (1.6)	-21.8 (1.4)	-21.0 (1.0)	-20.1 (1.2)		
	Median	-20.7	-21.9	-20.9	-20.3	21	0.0001
δ^{15}N-PN	Min, Max	1.8, 7.5	1.9, 6.3	3.8, 7.0	1.0, 6.5		
	Mean (SD)	4.2 (1.3)	4.0 (1.3)	5.1 (0.7)	4.8 (1.2)		
	Median	4.2	3.8	5.1	5.2	14.7	0.002
DOC	Min, Max	66.0, 85.6	65.9, 108	62.6, 77.2	55.4, 91.1		
	Mean (SD)	74.8 (4.9)	84.6 (9.7)	69.3 (3.4)	77.9 (7.1)		
	Median	73.6	84.3	69.1	77.9	55.1	<0.0001
DON	Min, Max	4.6, 11.7	4, 9.7	2.9, 8.9	5.9, 16.6		
	Mean (SD)	7.1 (1.7)	7.1 (1.4)	6.5 (1.5)	8.7 (2.6)		
	Median	7.1	7.2	6.6	7.8	12.6	0.0057
DOP	Min, Max	<0.01, 0.39	<0.01, 0.13	0.03, 0.42	<0.01, 0.5		
	Mean (SD)	0.12 (0.08)	0.03 (0.03)	0.13 (0.10)	0.15 (0.09)		
	Median	0.12	0.02	0.11	0.14	49.8	<0.0001
DOC:DON ratio	Min, Max	6.9, 17.3	7.7, 19.4	7.9, 23.5	3.8, 13		
	Mean (SD)	11.1 (2.47)	12.4 (2.70)	11.6 (4.05)	9.7 (1.98)		
	Median	10.8	12.0	10.1	10.3	16.0	0.0011
DON:DOP ratio	Min, Max	18.6, 681	38.9, 1800	18.1, 146	49.4, 98.9		
	Mean (SD)	111 (150)	309 (366)	63.8 (42.9)	63.9 (15.2)		
	Median	59.6	155	46.3	62.1	26.7	<0.0001
Chl-a (CTD- and filter data)	Min, Max	0.43, 1.72	0.38, 2.55	0.56, 2.60	0.27, 2.39		
	Mean (SD)	0.89 (0.31)	0.97 (0.46)	1.42 (0.65)	1.17 (0.58)		
	Median	0.84	0.88	1.32	1.01	9.22	0.0266

Table 1. Summary values of physical and biogeochemical properties by season. χ^2- and p-values show results of Kruskal-Wallis tests for differences between seasons (all d.f. = 3).

359 *3.3 Dissolved and particulate organic matter and stable isotope ratios*

360 DOC showed a clear seasonal cycle with a typical peak of 80–100 μmol l^{-1} during both the
361 SW and the NE monsoon, and lower values (usually 65–70 μmol l^{-1}) during the intermonsoon
362 seasons (Fig. 4a,b). DON showed less clear seasonality, ranging mostly between 4–12 μmol
363 l^{-1}, but was slightly and significantly higher during the NE monsoon (Fig. 4c,d). In contrast,
364 DOP had clear seasonal variation, with very low concentrations during the SW monsoon
365 (when DOP was sometimes not detected) and a peak of ~0.1–0.2 μmol l^{-1} during the
366 intermonsoon and NE monsoon periods (Fig. 4e,f).
367 Unlike the dissolved nutrients, particulate nutrient concentrations had limited seasonal
368 variation, with concentrations ranging mostly between 7–20 μmol l^{-1} for POC, 1–4 μmol l^{-1}
369 for PN, and PP between 0.025–0.2 μmol l^{-1} (Fig. 4g–l). The values of all particulate
370 concentrations were very similar between both sites. However, the concentrations of all three
371 were significantly lower during the SW monsoon and higher during either the intermonsoon
372 or the NE monsoon periods (Fig. 4h,j,l; Table 1). The chlorophyll-*a* concentration ranged
373 mostly between 0.5–2.5 μg l^{-1} with an overall mean of 1.1 ± 0.52 μg l^{-1} (Fig. 4m). Filter-
374 based chlorophyll-*a* concentrations agreed with the Valeport FastCTD fluorometer with root
375 mean squared error = 0.51 μg l^{-1} (Fig. S3). Combining the Valeport data and the filter-based
376 data showed that chlorophyll-*a* was on average slightly but significantly elevated during
377 intermonsoon 2 (Fig. 4n; Table 1).
378

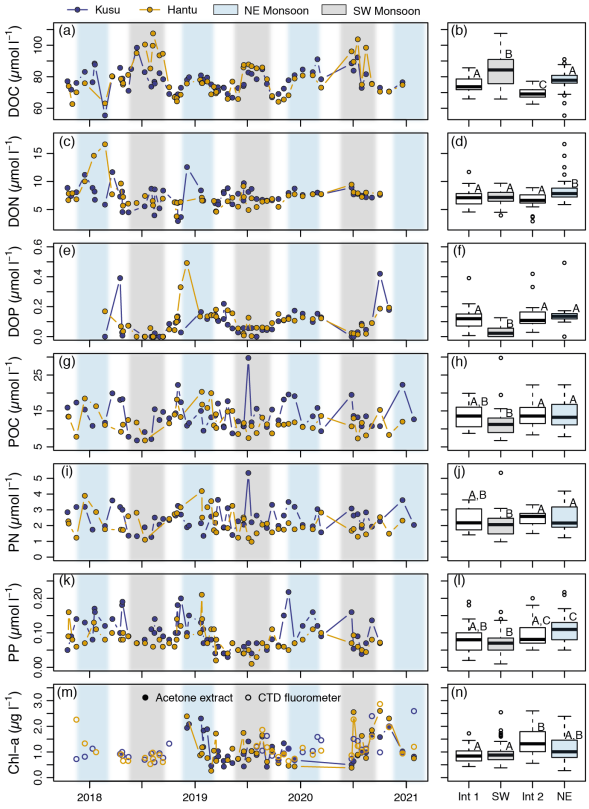

Fig. 4. Time series and seasonal boxplots of dissolved and particulate organic matter and chlorophyll-*a* concentrations. Colour shading and boxplot labelling are as for previous figures. Panel (m) shows data both from filter samples measured after acetone extraction and *in-vivo* measurements from the Valeport FastCTD fluorometer. The boxplot in panel (n) includes the fluorometer data for dates when no filter-based measurements are available.

δ^{13}C-POC ranged between -24.8‰ to -17.1‰, while δ^{15}N-PN ranged between +1.0‰ to +7.5‰; both showed moderate but significant differences between seasons, with lower values during the SW monsoon (Fig. 5a–d; Table 1). δ^{13}C-DIC showed an extremely clear seasonal cycle, ranging mostly from -1.5‰ to +0.5‰, with low values during the SW monsoon and high values during all other seasons (Fig. 5e,f). δ^{15}N-NO_x^- varied between +2.6‰ to +8.5‰ while δ^{18}O-NO_x^- ranged from -0.3‰ to +9.0‰ (Fig. 5g). NO_3^- concentrations were only sufficiently high during the SW and early NE monsoon to allow the isotopic composition to be measured; hence we did not test for seasonality. However, the three measurements from

the NE monsoon had the lowest $\delta^{15}N$ values. There was no significant relationship between $\delta^{18}O\text{-}NO_x^-$ and $\delta^{15}N\text{-}NO_x^-$, and the values could be consistent with either marine or terrestrial NO_3^- sources (Fig. 6).

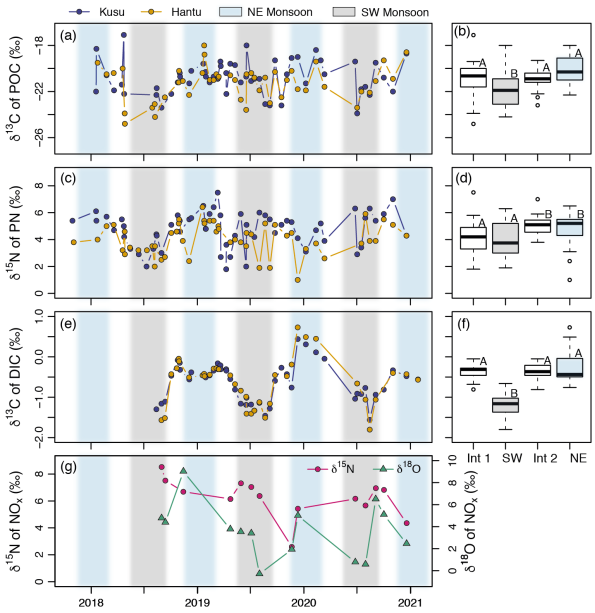

Fig. 5. Time series and seasonal boxplots of the isotopic composition ($\delta^{13}C$ and $\delta^{15}N$) of (a–d) particulate organic matter, and (e,f) dissolved inorganic carbon. Time series of $\delta^{15}N$ and $\delta^{18}O$ of NO_x^- (measured only at Kusu) is shown in (g). Since NO_x^- isotopes were only measured for dates with sufficiently high NO_3^- concentration, the seasonality was not analysed. Colour shading and boxplot labelling are as for previous figures.

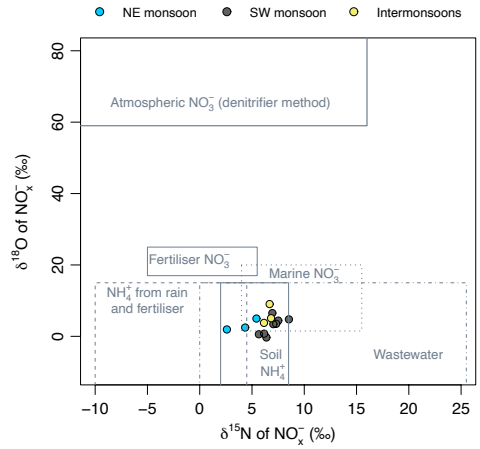

Fig. 6. Isotopic composition of dissolved NO_x^- at Kusu Island, together with approximate ranges of the main potential nitrogen sources drawn according to Kendall et al. (2007).

3.4 Nutrient stoichiometry and relationships between parameters

Regression statistics between parameters are given in Table 2. Dissolved inorganic nitrogen (DIN) showed a strong relationship to dissolved PO_4^{3-} that was close to the canonical Redfield ratio of 16:1, but with a tendency towards excess PO_4^{3-} (Fig. 7a). DIN was also closely related to $Si(OH)_4$, but with a considerable excess of silicon: the DIN:$Si(OH)_4$ ratio was invariably lower than 1, and the regression slope was 0.30 (Fig. 7b). POC and PN also showed a strong relationship that was close to the 6.6:1 Redfield stoichiometry (Fig. 7c),

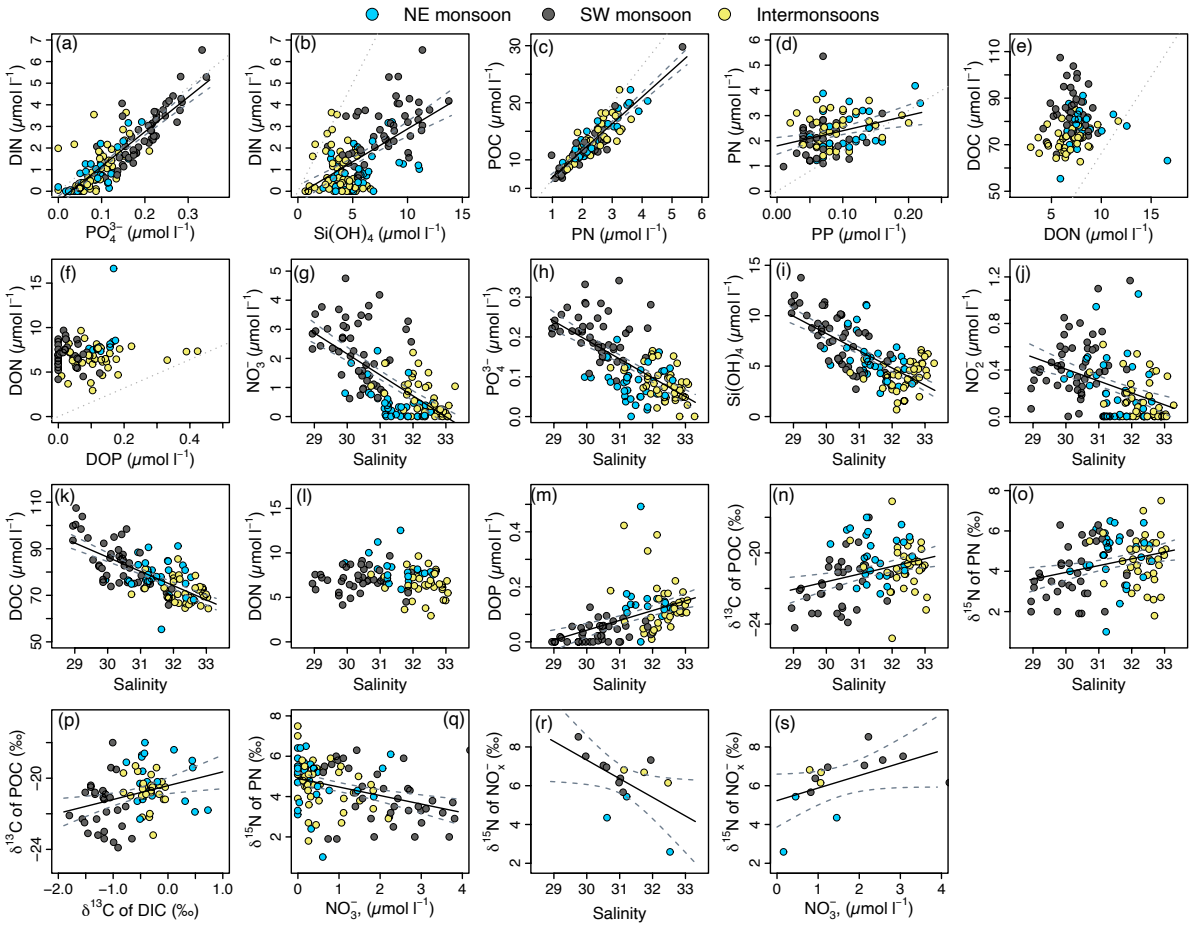

Fig. 7. Scatter plots between parameters to test for relationships and stoichiometric ratios. Solid black lines with dark-grey dashed lines indicate linear regression slopes with 95% confidence intervals; for regression parameters, see Table 2. Dotted grey lines in panels a–f indicate the canonical Redfield ratios (C:N:P = 106:16:1, N:Si = 1:1).

420 while PN and PP were less strongly related, with an N:P ratio above Redfield (mean of 33 ±
421 20 mol mol^{-1}; Fig. 7d). There was also no strong relationship between DOC and DON (Fig.
422 7e) or DON and DOP (Fig. 7f); the DOC:DON ratio was enriched in carbon relative to the
423 Redfield value of 6.6, while the DON:DOP ratio was enriched in nitrogen relative to the
424 Redfield value of 16 (Fig. 7e,f). Neither the POC:PN nor the PN:PP ratio showed significant
425 seasonal variation, but both the DOC:DON and the DON:DOP ratio were significantly higher
426 during the SW monsoon than at other times (Table 1). There was no significant relationship
427 between POC and chlorophyll-*a* concentration, and the POC:chlorophyll-*a* ratio was on
428 average relatively high (mean of 182 ± 113 g g^{-1}).
429

Parameters (y *versus* x)	Slope estimate (SE)	Intercept estimate (SE)	Statistics
DIN *versus* PO_4^{3-}	16.0 (0.77)	-0.45 (0.11)	r^2= 0.753, p<0.0001
DIN *versus* $Si(OH)_4$	0.304 (0.035)	-0.16 (0.22), NS	r^2=0.355, p<0.0001
POC *versus* PN	4.69 (0.22)	2.26 (0.53)	r^2=0.819, p<0.0001
PN *versus* PP	6.03 (1.74)	1.80 (0.17)	r^2=0.111, p<0.001
NO_3^- *versus* salinity	-0.720 (0.068)	23.7 (2.16)	r^2=0.461, p<0.0001
PO_4^{3-} *versus* salinity	-0.047 (0.004)	1.61 (0.139)	r^2=0.467, p<0.0001
$Si(OH)_4$ *versus* salinity	-1.71 (0.15)	59.5 (4.80)	r^2=0.494, p<0.0001
NO_2^- *versus* salinity	-0.102 (0.020)	3.48 (0.61)	r^2=0.176, p<0.0001
DOC *versus* salinity	-6.31 (0.581)	276 (18.2)	r^2=0.504, p<0.0001
DOP *versus* salinity	0.0358 (0.007)	-1.034 (0.221)	r^2=0.214, p<0.0001
δ^{13}C-POC *versus* salinity	0.432 (0.132)	-34.6 (4.15)	r^2=0.102, p<0.01
δ^{15}N-PN *versus* salinity	0.336 (0.112)	-6.12 (3.53), NS	r^2=0.081, p<0.01
δ^{15}N-NO_x^- *versus* salinity	-0.961 (0.422)	36.1 (13.1)	r^2=0.302, p<0.05
pH anomaly *versus* dissolved O_2 anomaly (10-min frequency)	$1.705*10^{-3}$ ($7.95*10^{-6}$)	$-1.883*10^{-5}$ ($5.606*10^{-5}$), NS	r^2=0.653, p<0.0001
Diel pH change *versus* diel dissolved O_2 change	$1.079*10^{-3}$ ($1.25*10^{-4}$)	0.0288 (0.0045)	r^2=0.299, p<0.0001

430

431 Table 2. Results of regression analyses for relationships between key biogeochemical and physical parameters.
432 Intercepts that are not statistically significant are marked NS. p-values refer to the significance of the regression
433 slopes.

434 NO_3^-, PO_4^{3-}, and $Si(OH)_4$, and to a lesser degree NO_2^-, all showed strong inverse relationships
435 with salinity (Fig. 7g–j). This was also clearly seen for DOC, but not for DON (which
436 seemed to show a unimodal relationship), while DOP was positively related to salinity, but
437 with high variability (Fig. 7k–m). POC, PN, and PP did not show significant relationships to
438 salinity (not shown), but both δ^{13}C-POC and δ^{15}N-PN were weakly related to salinity (Fig.
439 7n,o). Consequently, δ^{13}C-POC and δ^{15}N-PN were also weakly related to δ^{13}C-DIC and NO_3^-
440 concentrations, respectively (Fig. 7p,q). δ^{15}N-NO_x^- showed a clear inverse relationship to
441 salinity and consequently a positive relationship with NO_3^- concentrations (Fig. 7r,s).
442 Parameters that were significantly related to salinity were also significantly related to CDOM
443 (as a_{350}), mostly with equal or slightly higher r^2 values (Fig. S4; Table S1).
444
445 *3.5 Dissolved O_2 and pH dynamics*
446 Seawater pH varied mostly between 7.80–8.05, showing appreciable high-frequency
447 variability. Moreover, there was a strong seasonal difference in daily mean pH, with lowest
448 values during the SW monsoon (Fig. 8a,b, Table 1). In contrast, dissolved O_2 chiefly showed
449 high-frequency variability between typically 150–210 µmol l^{-1} (Fig. 8c). Although seasonal
450 differences in daily mean dissolved O_2 were technically significant, their magnitude was too
451 small to be environmentally relevant (<5 µmol l^{-1} difference in medians; Fig. 8d, Table 1).
452 Plotting the daily anomaly of pH and dissolved O_2 against time revealed a clear diel cycle
453 with a minimum at 05:30–06:30 local time and a maximum at 14:00–15:00; the average diel
454 change was 0.022 pH units and 14.2 µmol O_2 l^{-1} (Fig. 8e,f). There was a strong relationship
455 between the pH and dissolved O_2 anomalies at 10-min frequency (Fig. 8g), and a relationship
456 between the diel change in pH and dissolved O_2 (Fig. 8h). The diel variation in both pH and
457 of dissolved O_2 showed some evidence of seasonal variability, with diel pH change greatest

458 during the SW and lowest during the NE monsoon, and diel dissolved O_2 change greatest
459 during intermonsoon 1 and lowest during the NE monsoon (Fig. 8i–l, Table 1).
460
461

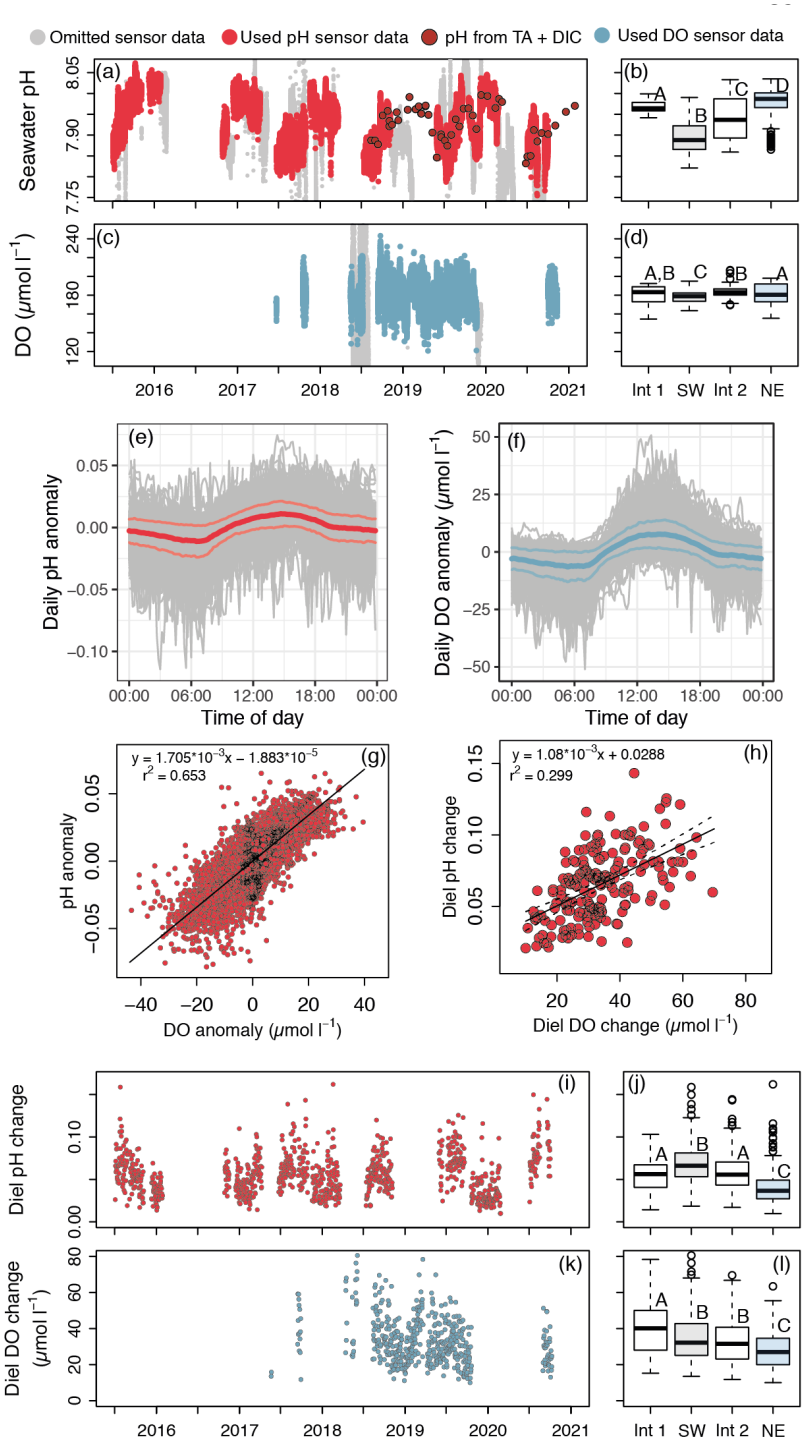

Fig. 8. Time series and seasonal boxplots of (a,b) seawater pH and (c,d) dissolved O_2 at Kusu. Diel anomalies of (e) seawater pH and (f) dissolved O_2; grey lines show individual daily data, solid blue and red lines show overall mean ± standard deviation. Relationships between (g) individual diel anomalies in pH and dissolved O_2 at 10-min frequency, and (h) between the maximum diel change in pH and dissolved O_2 (on point for each day). Solid black and dashed grey lines indicate linear regression with 95% confidence interval. Time series and seasonal boxplots of maximum diel change in (i,j) seawater pH and (k,l) dissolved oxygen. Monsoon shading in the time series has been omitted for clarity; boxplot labelling is as for previous figures.

4. Discussion

4.1 Seasonality and range in dissolved nutrient concentrations

Dissolved inorganic nutrient concentrations have rarely been reported from the Singapore Strait, and only for shorter time periods and/or with lower measurement frequency. The values we measured are broadly consistent with previous studies (Browne et al., 2015; Chénard et al., 2019; Deignan and McDougald, 2021; Gin et al., 2000), which also noted that dissolved nutrient concentrations are typically elevated during the SW monsoon. Our data clearly show that the Singapore Strait undergoes strong and consistent seasonal variation from low concentrations typical of oligotrophic waters (especially during and after the late NE monsoon) to significantly higher values during the SW monsoon (Fig. 3). Our nutrient concentrations during the late NE monsoon and intermonsoon 1 are similar to reports from the open Sunda Shelf and the South China Sea (Kartadikaria et al., 2015; Liu et al., 2020; Ning et al., 2004). In contrast, nutrient concentrations during the SW monsoon are similar to values reported from the Malacca Strait (Lim et al., 2021; Lim et al., 2015). However, chlorophyll-*a* concentrations were above 0.4 μg l^{-1} in all but two samples, with an average of about 1 μg l^{-1} (Fig. 4). This is greater than reported from the open Sunda Shelf Sea (Kartadikaria et al., 2015; Ke et al., 2014; Liu et al., 2020), and indicates that the Singapore Strait does not experience genuinely oligotrophic conditions, even when dissolved inorganic nutrients are low. For comparison, eutrophication thresholds for coral reefs are typically considered to be ~1 μmol l^{-1} DIN, 0.1–0.2 μmol l^{-1} PO_4^{3-}, and 0.2–0.4 μg l^{-1} chlorophyll-*a* (Bell, 1992; Bell et al., 2014).

The dissolved organic matter pool showed a somewhat different seasonal pattern. While DOC showed similar seasonality to the inorganic nutrients, as described previously (Zhou et al., 2021), the DON concentration showed very limited seasonal changes, and the DOP

concentration showed an opposite seasonal pattern, with lowest concentrations during the SW monsoon and highest during the NE and intermonsoon (Fig. 4). The DOC and DON concentrations are similar to those in other coastal locations in the tropical Indo-Pacific (Kuwahara et al., 2010; Lønborg et al., 2021a; Martin et al., 2018). The DOP concentrations in Singapore are lower than reported from the Great Barrier Reef by Lønborg et al. (2021a) (average of 0.21 ± 0.16 μmol l^{-1}), but similar to recent reports from coastal locations around the Malay Peninsula (Lim et al., 2018) (average of 0.07 ± 0.03 μmol l^{-1}). The fact that DOP was sometimes undetectable during the SW monsoon (i.e. the total dissolved P concentration was equal to the dissolved PO_4^{3-} measurement) might indicate that a refractory DOP fraction was incompletely oxidised, or alternatively that a labile DOP fraction was hydrolysed during dissolved PO_4^{3-} measurements. However, the close agreement between our two sites and consistent seasonal patterns between years clearly suggest that at least the relative variation in DOP is accurate.

Overall, and taken together with the strong seasonality in salinity (Fig. 2), our results confirm that dissolved biogeochemical properties in the Singapore Strait are largely controlled by the regional advection of distinct water masses according to the monsoon-driven changes in ocean currents, as previously described for DOC and for coloured dissolved organic matter (Martin et al., 2021; Zhou et al., 2021). Our data also provide further support for classifying the Singapore Strait as a mesotrophic environment (Lim et al., 2021) despite the seasonally low concentrations of inorganic nutrients.

4.2 Sources of nutrients

The strong inverse relationships of NO_3^-, PO_4^{3-}, and $Si(OH)_4$ to salinity (Fig. 7) clearly indicate a terrestrial source from regional river input. Using stable carbon isotopes, Zhou et al. (2021) demonstrated that a large fraction of DOC in the Singapore Strait during the SW

monsoon originates from regional peatlands. The fact that all three nutrients were more strongly correlated with CDOM than with salinity (as seen by the higher r^2 values; Fig. S4) provides further support for a predominantly terrestrial source of nutrients in the Singapore Strait, as CDOM is a good tracer of terrestrial DOC in the Sunda Shelf Sea (Martin et al., 2018; Martin et al., 2021; Mizubayashi et al., 2013; Siegel et al., 2019).

The intercepts of our nutrient–salinity regressions can be taken as estimated riverine end-member concentrations. This implies average river concentrations of 23.7 ± 2.2 μmol l^{-1} for NO_3^-, 1.61 ± 0.14 μmol l^{-1} for PO_4^{3-}, and 59.5 ± 4.8 μmol l^{-1} for $Si(OH)_4$ (Fig. 7, Table 2). This is at the low end of $Si(OH)_4$ concentrations in small tropical rivers in Asia (Jennerjahn et al., 2006), and our inferred riverine end-member values of all three nutrients are several-fold lower than reported from human-impacted river systems on Java (Damar et al., 2019; Jennerjahn et al., 2004). Tropical peatland-draining rivers carry low nutrient concentrations, often <5 μmol l^{-1} DIN, unless they are affected by anthropogenic nutrient inputs (Alkhatib et al., 2007; Baum, 2008), consistent with efficient nutrient retention within the peatland ecosystem (Mishra et al., 2021). However, our inferred riverine end-member concentrations are well within the range reported for peatland-draining rivers with varying degrees of anthropogenic impact from Sumatra and Borneo (Alkhatib et al., 2007; Bange et al., 2019; Baum, 2008; Gandois et al., 2020; Jiang et al., 2019).

The fact that NO_2^- was only weakly related to salinity and CDOM (Fig. 7), while NH_4^+ was unrelated to salinity and was consistently low during the SW monsoon (Fig. 3), suggests that these two nitrogen species originate primarily from internal recycling, rather than being derived directly from land. NO_2^- and NH_4^+ concentrations in peatland rivers have only been reported from the Siak and Rajang rivers, where NO_2^- is typically <0.5 μmol l^{-1} but NH_4^+ is usually 2–15 μmol l^{-1} (Baum, 2008; Jiang et al., 2019). Our data therefore suggest that riverine NH_4^+ is rapidly transformed in the estuaries and coastal waters, likely through a

562 combination of phytoplankton uptake and nitrification, as also noted along the salinity
563 gradient of the Rajang delta on Borneo (Jiang et al., 2019). Recycling of organic nitrogen
564 (either terrestrial or aquatic in origin) by ammonification followed by nitrification could also
565 act as a source of NO_2^- in coastal waters. In subtropical coastal waters of North America,
566 temperature-dependent NO_2^- accumulation can occur when NH_4^+ oxidation and NO_2^-
567 oxidation become uncoupled between 20–30°C, owing to the different temperature
568 sensitivities of the microbial taxa responsible for each of these nitrification steps (Schaefer
569 and Hollibaugh, 2017). Whether the permanently high temperatures in tropical coastal waters
570 might promote NO_2^- accumulation over complete nitrification may be worth testing in future
571 research, especially in the context of increasing tropical surface temperatures. Since the water
572 column at our site was always oxygenated (Fig. 8), it is unlikely that hypoxia was mediating
573 nitrification rates (Schaefer and Hollibaugh, 2017).
574 The δ^{15}N-NO_x^- and δ^{18}O-NO_x^- values are slightly higher compared to values measured in the
575 Rajang River in northwest Borneo (Jiang et al., 2019), but do not provide an unambiguous
576 source fingerprint (Fig 6; (Kendall et al., 2007)). Although the isotopic composition could be
577 consistent with marine NO_3^-, this is only plausible for the NE monsoon period, given the
578 strong inverse relationship of NO_3^- concentration with salinity. For the SW monsoon, the
579 isotopic data would be consistent with soil N, wastewater, or a combination of fertiliser and
580 wastewater (Fig. 6). Most of the peatlands on Sumatra are used for agriculture and have
581 synthetic fertilisers applied regularly; Baum (2008) reported that fertilisers and wastewater
582 are the main nutrient sources to the Siak, which is one of the main river systems on Sumatra.
583 Although atmospheric deposition was suggested previously to be a significant source of NO_3^-
584 to the Singapore Strait (Sundarambal et al., 2010), our isotope data are not consistent with a
585 significant contribution from atmospheric NO_3^- deposition during any season. The monthly
586 mean δ^{15}N- and δ^{18}O- NO_3^- values in rainfall in Singapore are nearly all <2‰ and >50‰,

respectively (Li et al., 2020). The fact that δ^{15}N-NO_x^- during the NE monsoon had the lowest values measured, even below typical marine NO_3^- values (Fig. 6) may point to a significant contribution from N fixation: the shallow subsurface NO_3^- pool in the South China Sea is isotopically depleted due to diazotrophy (Ren et al., 2017; Zhang et al., 2020), and additional N fixation is likely to take place across the Sunda Shelf Sea. For example, N fixation was reported from the Singapore Strait even during the DIN-rich SW monsoon, both in the water column and associated with corals, albeit at relatively low rates (Moynihan et al., 2021).

In contrast to the main inorganic nutrients and to DOC, neither DON nor DOP appeared to have a predominant terrestrial source, given their different seasonal patterns (Fig. 4). While very low DOP concentrations during the SW monsoon might seem surprising, this provides further support for the view that peatlands are the main source of river run-off influencing the Singapore Strait during the SW monsoon (Zhou et al., 2021). Tropical peatlands are ombrotrophic, nutrient-poor systems that retain nutrients efficiently and can become particularly phosphorus-poor, while nitrogen-fixing vegetation continues to provide a nitrogen source even in old peatlands (Mishra et al., 2021; Troxler, 2007). Hence, the most likely explanation for the DON and DOP dynamics is that the DOP is predominantly of marine origin (and is hence high during the NE monsoon and intermonsoon months), while the DON has both significant marine and terrestrial sources, and hence shows little seasonality. Measurements of both DON and DOP in peatland-draining rivers would be valuable to clarify this further. While disturbed peatlands converted to agricultural use can clearly be a source of inorganic nutrients through fertiliser input, as reflected in our inorganic nutrient data, the dissolved organic matter exported from disturbed peatlands consists of increasingly old soil organic matter (Evans et al., 2014), which would explain the different dynamics of the inorganic and the organic nutrients at our site.

611 At present, the bioavailability of DON and DOP in the Sunda Shelf Sea is unknown. In the
612 Great Barrier Reef, DON and DOP contributed more bioavailable N and P than either
613 dissolved inorganic or particulate nutrients (Lønborg et al., 2018), but the DOM pool in that
614 study was predominantly of marine origin. In the open South China Sea, isotopic evidence
615 points to active DON cycling with DON production and remineralization rates approximately
616 in balance (Zhang et al., 2020). However, peatland-derived DOC in Southeast Asia appears to
617 be relatively refractory to direct remineralisation by heterotrophic microbes, even when
618 inorganic N and P are added (Nichols and Martin, 2021), suggesting that the terrestrial
619 organic nutrient pools might also be relatively refractory. Nevertheless, the majority of this
620 peatland DOC is ultimately remineralised before leaving the Sunda Shelf (Wit et al., 2018;
621 Zhou et al., 2021), although the biogeochemical processes driving this remineralisation
622 remain unclear. If peatland DON is also remineralised to a similar degree as DOC in the
623 Sunda Shelf, then given the relative lack of DOP, this might lead to an imbalanced N:P ratio
624 in areas receiving peatland run-off. Interestingly, the N:P stoichiometry of the particulate
625 pool is typically higher than the canonical Redfield ratio of 16:1 (Fig. 7), although this might
626 also reflect a contribution from detrital organic matter to the particulate pool (see Section
627 4.3). The Singapore Strait also has measurable alkaline phosphatase activity year-round
628 (Nichols et al., submitted manuscript), suggesting that least a fraction of DOP is actively
629 cycled. Resolving the bioavailability of both the terrestrial and marine DON and DOP pools
630 will be important both for understanding the patterns of primary productivity in this region,
631 and to reach a more complete understanding of how land use-driven changes in terrestrial
632 DOM fluxes (Moore et al., 2013) affect coastal seas.
633
634 *4.3 Composition and dynamics of particulate organic matter*

635 The fact that the particulate organic matter pool and the chlorophyll-*a* concentration showed
636 only relatively limited seasonality and did not directly follow the seasonal cycle in inorganic
637 nutrients indicates that phytoplankton biomass is not primarily controlled by nutrient
638 availability. Even during the low-nutrient intermonsoon periods, chlorophyll-*a* was usually
639 >0.5 µg l^{-1}, which suggests that nutrients are efficiently recycled during these periods to
640 maintain phytoplankton productivity and standing stock. This is consistent with the
641 observation of year-round measurable levels of alkaline phosphatase activity in the water
642 column, averaging 9 nmol l^{-1} h^{-1}, most likely from heterotrophic microbial sources (Nichols
643 et al., submitted manuscript). However, chlorophyll-*a* was on average elevated during
644 intermonsoon 2 and partly also during the NE monsoon (Fig. 4). This does suggest that the
645 SW monsoon nutrient input stimulates a delayed phytoplankton growth response. The delay
646 might be linked to greater light limitation during the SW monsoon due to the presence of
647 peatland CDOM, which leads to shoaling of the euphotic zone and changes in the spectral
648 quality of light underwater (Martin et al., 2021). Phytoplankton production in tropical and
649 subtropical estuaries experiencing episodic nutrient delivery is similarly thought to be
650 modulated by light limitation from high turbidity during flood events (Burford et al., 2012;
651 Eyre, 2000), and depth-integrated phytoplankton productivity along the Great Barrier Reef is
652 consistently greater at offshore stations with greater light availability (Furnas et al., 2005).
653 However, this apparent seasonal increase in chlorophyll-*a* concentration was small and not
654 consistent between years, e.g. no increase was seen in 2019 (Fig. 4). It is probable that
655 grazing, especially by microzooplankton, is also a key factor controlling phytoplankton
656 biomass, as noted, for example, in Darwin Harbour and the Great Barrier Reef (Burford et al.,
657 2008; Furnas et al., 2005).
658 Although the POC:PN ratio was very close to the Redfield ratio, the PN:PP ratio was higher
659 (Fig. 7), and the POC:chlorophyll-*a* ratio was greater than might be expected for

660 phytoplankton biomass in the relatively low-light environment of the Singapore Strait
661 (Arteaga et al., 2016; Geider et al., 1997). This suggests that a significant part of the
662 particulate organic matter pool was likely detrital. Whether the detrital POM fraction is
663 primarily from marine production or originates from terrestrial input is unclear: the overall
664 mean δ^{13}C-POC (-21.0 ± 1.5‰) is compatible with a purely marine origin (Fry and Sherr,
665 1989; Verwega et al., 2021), but the small decrease in δ^{13}C-POC during the SW monsoon
666 (Fig. 5) might indicate a contribution of terrestrial POC during this period. However, the
667 strong decrease in δ^{13}C-DIC during the SW monsoon, caused by peatland DOC
668 remineralisation (Zhou et al., 2021), means that this might also reflect phytoplankton carbon
669 assimilation from a more isotopically depleted DIC pool (Chanton and Lewis, 1999). The
670 δ^{15}N-PN data don't help to resolve this question, as δ^{15}N-PN in Sumatran peatland rivers
671 appears to be mostly in the range of +2‰ to +6‰ (Alkhatib et al., 2007; Baum, 2008),
672 essentially the same as our data.
673
674 *4.4. Net community metabolism*
675 Net community metabolism causes correlated diel changes in pH and dissolved O_2, as seen in
676 Fig. 8. On corals reefs, such variation is driven by a combination of photosynthesis–
677 respiration and calcification–carbonate dissolution (Albright et al., 2015; DeCarlo et al.,
678 2017; Page et al., 2019). These previous studies were typically conducted on extensive reef
679 flats with limited water exchange, and they consequently observed larger changes, with diel
680 variation in pH mostly ≥0.1 unit and in dissolved O_2 ≥50 µmol l^{-1}. In our case, the sensors
681 were installed along a reef slope exposed to the open sea, and the coral reef only extends
682 about 20 m from the shoreline. Therefore, the variation in our dataset is most likely
683 dominated by planktonic photosynthesis and respiration rather than by benthic metabolism
684 and calcification.

The diel change in dissolved O_2 varied by a factor of 3–4 within each season, but was on average highest during intermonsoon 1 and lowest during the NE monsoon (Fig. 8). This pattern suggests that light availability is an important control over primary productivity: Singapore experiences lower rainfall and more solar radiation during the late NE and intermonsoon 1 than in other seasons (Fong, 2012), while CDOM input during the SW monsoon (and to a lesser degree during the early NE monsoon) increases the absorption of sunlight underwater, especially at blue wavelengths (Martin et al., 2021). At the same time, suspended matter concentrations can vary substantially over short (<1 day) periods on reefs in Singapore (Morgan et al., 2020), further contributing to variation in light attenuation and therefore productivity rates within seasons.

Our data therefore indicate that phytoplankton productivity in the Singapore Strait is likely more limited by light than by nutrient availability. While this would imply that increases in nutrient input might not trigger phytoplankton blooms, the tendency for chlorophyll-*a* to increase after the SW monsoon nutrient input (Fig 6) suggests that phytoplankton biomass might still respond to increases in nutrients. This could be the case especially during the low-nutrient intermonsoon periods, when CDOM concentrations are lower. Increases in nutrient concentrations, such as from future aquaculture expansion (Tan, 2020) or from increased riverine supply, might therefore still cause further eutrophication in the strait. Continued monitoring is hence warranted. Our inorganic nutrient data point towards potential N- rather than P-limitation, but also reveal an excess of $Si(OH)_4$ over N (Fig. 7). This is consistent with observed chlorophyll-*a* increases in experimental incubations of Singapore Strait water upon N addition (Gin et al., 2006), and the fact that diatoms are consistently a large fraction of the phytoplankton community (Chénard et al., 2019; Gin et al., 2006).

The fact that the diel change in pH does not follow the same seasonal pattern as dissolved O_2, but is on average highest during the SW monsoon (Fig. 8), reflects the seasonal change in the

710 mean state of the carbonate system: the low salinity during the SW monsoon means that total
711 alkalinity is lower than during other seasons, while peatland DOC remineralisation leads to a
712 relative excess of DIC (Zhou et al., 2021). Consequently, the buffering capacity is lowest
713 during the SW monsoon, and so the diel change in pH for a given change in dissolved CO_2
714 concentration due to metabolic processes is necessarily larger (Pacella et al., 2018). In
715 contrast, the low diel pH variation during the NE monsoon results from both the higher
716 buffering capacity and the lower net community metabolism at this time. Marine ecosystems
717 in this part of the Sunda Shelf might therefore be more vulnerable to future ocean
718 acidification, because the seawater buffering capacity will be depleted both by uptake of
719 atmospheric CO_2 across the South China Sea and further by terrigenous DOC
720 remineralisation on the shelf (Zhou et al., 2021). We therefore expect that the diel variation in
721 the carbonate system will increase further, especially during the SW monsoon. Such diel
722 carbonate system variation due to community respiration can lead to periods of net $CaCO_3$
723 dissolution on reefs, especially from the reef sediment (Stoltenberg et al., 2021). Coral reefs
724 in the Singapore Strait already have relatively low net $CaCO_3$ accretion rates and low vertical
725 accretion potential even without considering possible sedimentary dissolution (Januchowski-
726 Hartley et al., 2020). Future ocean acidification of the incoming open-ocean water is
727 therefore an important potential threat to these reefs.
728
729
730 **5. Conclusions**
731
732 Our results show that terrestrial input is a major source of dissolved inorganic nutrients to the
733 central Sunda Shelf, with coastal waters characterised by DIN:PO_4^{3-} ratios close to or slightly
734 below the Redfield ratio, and an excess of dissolved Si over DIN. The source of nutrients is

likely a combination of natural input from soils together with fertiliser and wastewater input, but atmospheric deposition appears to be at most minor. Rivers additionally provide a major input of peatland-derived dissolved organic matter to coastal waters, although this input is notably poor in DOP. The Singapore Strait experiences strong seasonal variation because the semi-annual current reversal advects either terrestrially influenced water masses or water from the open South China Sea through the Strait. The particulate organic matter pool shows far less seasonal variation, suggesting a greater control from local production within coastal waters and possibly resuspension from the sediment. While there is likely a significant detrital contribution to the particulate organic matter pool, phytoplankton biomass is higher than would be expected for genuinely oligotrophic tropical waters. Phytoplankton productivity is probably limited more by light than by nutrients, but phytoplankton biomass does appear to increase in response to seasonal nutrient inputs, at least in some years. Net community metabolism causes stronger diel variation in pH during the SW monsoon than in other seasons, when terrigenous DOC remineralisation depletes the buffering capacity. This metabolic feedback, in combination with the impact of terrigenous DOC remineralisation, may render marine ecosystems in this region of Southeast Asia more vulnerable to the future effects of ocean acidification.

Acknowledgements

We are very grateful to the many colleagues and students who helped with field and laboratory work, especially Nikita Kaushal, Kyle M. Morgan, and Nathalie F. Goodkin. Francis Yeo and the crew of *Dolphin Explorer* were instrumental in supporting the field work. Isotope analysis at the University of Hong Kong was performed by Leung Kit Sum. This research was funded through the Marine Science Research and Development Programme and the Marine Environment Sensing Network of the National Research

760 Foundation, Singapore, Prime Minister's Office (grants MSRDP-P11, MSRDP-P32, and
761 NRF-NRI-2020-MESN), and was carried out under research permit NP/RP17-044-3 from the
762 Singapore National Parks Board.

763

764 Data availability

765 All data and analysis codes are archived in the Nanyang Technological University data
766 repository and can be accessed at https://doi.org/10.21979/N9/2FQEGW.

767

768 References
769
770 Albright, R., Benthuysen, J., Cantin, N., Caldeira, K., Anthony, K., 2015. Coral reef
771 metabolism and carbon chemistry dynamics of a coral reef flat. Geophys. Res. Lett. 42,
772 3980-3988.
773 Alkhatib, M., Jennerjahn, T.C., Samiaji, J., 2007. Biogeochemistry of the Dumai River
774 estuary, Sumatra, Indonesia, a tropical black-water river. Limnol. Oceanogr. 52, 2410-
775 2417.
776 Arteaga, L., Pahlow, M., Oschlies, A., 2016. Modeled Chl:C ratio and derived estimates of
777 phytoplankton carbon biomass and its contribution to total particulate organic carbon in
778 the global surface ocean. Glob. Biogeochem. Cycles 30, 1791-1810.
779 Bange, H.W., Sim, C.H., Bastian, D., Kallert, J., Kock, A., Mujahid, A., Müller, M., 2019.
780 Nitrous oxide (N_2O) and methane (CH_4) in rivers and estuaries of northwestern Borneo.
781 Biogeosciences 16, 4321-4335.
782 Baum, A., 2008. The Siak River in Central Sumatra, Indonesia. University of Bremen.
783 Baum, A., Rixen, T., Samiaji, J., 2007. Relevance of peat draining rivers in central Sumatra
784 for the riverine input of dissolved organic carbon into the ocean. Estuar. Coast. Shelf
785 Sci. 73, 563-570.
786 Bell, P.R.F., 1992. Eutrophication and coral reefs—some examples in the Great Barrier Reef
787 lagoon. Water Res. 26, 553-568.
788 Bell, P.R.F., Elmetri, I., Lapointe, B.E., 2014. Evidence of large-scale chronic eutrophication
789 in the Great Barrier Reef: quantification of chlorophyll a thresholds for sustaining coral
790 reef communities. Ambio 43, 361-376.
791 Browne, N.K., Tay, J.K.L., Low, J., Larson, O., Todd, P.A., 2015. Fluctuations in coral
792 health of four common inshore reef corals in response to seasonal and anthropogenic
793 changes in water quality. Mar. Environ. Res. 105, 39-52.
794 Brunskill, G.J., 2010. Tropical Margins, in: Liu, K.-K., Atkinson, L., Quiñones, R., Talaue-
795 McManus, L. (Eds.), Carbon and Nutrient Fluxes in Continental Margins: A Global
796 Synthesis. Springer Berlin Heidelberg, Berlin, Heidelberg, pp. 423-493.
797 Burford, M.A., Alongi, D.M., McKinnon, A.D., Trott, L.A., 2008. Primary production and
798 nutrients in a tropical macrotidal estuary, Darwin Harbour, Australia. Estuar. Coast.
799 Shelf Sci. 79, 440-448.

Burford, M.A., Webster, I.T., Revill, A.T., Kenyon, R.A., Whittle, M., Curwen, G., 2012. Controls on phytoplankton productivity in a wet–dry tropical estuary. Estuar. Coast. Shelf Sci. 113, 141-151.

Chai, X., Li, X., Hii, K.S., Zhang, Q., Deng, Q., Wan, L., Zheng, L., Lim, P.T., Tan, S.N., Mohd-Din, M., Song, C., Song, L., Zhou, Y., Cao, X., 2021. Blooms of diatom and dinoflagellate associated with nutrient imbalance driven by cycling of nitrogen and phosphorus in anaerobic sediments in Johor Strait (Malaysia). Mar. Environ. Res. 169, 105398.

Chanton, J.P., Lewis, F.G., 1999. Plankton and dissolved inorganic carbon isotopic composition in a river-dominated estuary: Apalachicola Bay, Florida. Estuaries 22, 575-583.

Chénard, C., Wijaya, W., Vaulot, D., Lopes dos Santos, A., Martin, P., Kaur, A., Lauro, F.M., 2019. Temporal and spatial dynamics of Bacteria, Archaea and protists in equatorial coastal waters. Sci. Rep. 9, 16390.

Damar, A., Hesse, K.-J., Colijn, F., Vitner, Y., 2019. The eutrophication states of the Indonesian sea large marine ecosystem: Jakarta Bay, 2001–2013. Deep Sea Res. II 163, 72-86.

DeCarlo, T.M., Cohen, A.L., Wong, G.T.F., Shiah, F.-K., Lentz, S.J., Davis, K.A., Shamberger, K.E.F., Lohmann, P., 2017. Community production modulates coral reef pH and the sensitivity of ecosystem calcification to ocean acidification. J. Geophys. Res. Oceans 122, 745-761.

Deignan, L.K., McDougald, D., 2021. Differential Response of the Microbiome of *Pocillopora acuta* to Reciprocal Transplantation Within Singapore. Microb. Ecol.

Dickson, A.G., 1990. Standard potential of the reaction: $AgCl(s) + 12H_2(g) = Ag(s) + HCl(aq)$, and and the standard acidity constant of the ion HSO_4^- in synthetic sea water from 273.15 to 318.15 K. J. Chem. Thermodyn. 22, 113-127.

Evans, C.D., Page, S.E., Jones, T., Moore, S., Gauci, V., Laiho, R., Hruška, J., Allott, T.E.H., Billett, M.F., Tipping, E., Freeman, C., Garnett, M.H., 2014. Contrasting vulnerability of drained tropical and high-latitude peatlands to fluvial loss of stored carbon. Glob. Biogeochem. Cycles 28, 1215-1234.

Eyre, B.D., 2000. Regional evaluation of nutrient transformation and phytoplankton growth in nine river-dominated sub-tropical east Australian estuaries. Mar. Ecol. Prog. Ser. 205, 61-83.

Fong, M., 2012. The Weather and Climate of Singapore. Meteorological Service Singapore, Singapore.

Fry, B., Sherr, E.B., 1989. $\delta^{13}C$ Measurements as Indicators of Carbon Flow in Marine and Freshwater Ecosystems, in: Rundel, P.W., Ehleringer, J.R., Nagy, K.A. (Eds.), Stable Isotopes in Ecological Research. Springer New York, New York, NY, pp. 196-229.

Furnas, M., Mitchell, A., Skuza, M., Brodie, J., 2005. In the other 90%: phytoplankton responses to enhanced nutrient availability in the Great Barrier Reef Lagoon. Mar. Pollut. Bull. 51, 253-265.

Gandois, L., Hoyt, A.M., Mounier, S., Le Roux, G., Harvey, C.F., Claustres, A., Nuriman, M., Anshari, G., 2020. From canals to the coast: dissolved organic matter and trace metal composition in rivers draining degraded tropical peatlands in Indonesia. Biogeosciences 17, 1897-1909.

Gattuso, J.P., Epitalon, J.-M., Lavigne, H., 2016. seacarb: Seawater Carbonate Chemistry. R package version 3.1.1. https://CRAN.R-project.org/package=seacarb.

Geider, R.J., MacIntyre, H.L., Kana, T.M., 1997. Dynamic model of phytoplankton growth and acclimation: responses of the balanced growth rate and the chlorophyll a:carbon ratio to light, nutrient-limitation and temperature. Mar. Ecol. Prog. Ser. 148, 187-200.

Gin, K.Y.-H., Holmes, M.J., Zhang, S., Lin, X., 2006. Phytoplankton Structure in the Tropical Port Waters of Singapore, in: Wolanski, E. (Ed.), The Environment in Asia Pacific Harbours. Springer Netherlands, Dordrecht, pp. 347-375.

Gin, K.Y.-H., Lin, X., Zhang, S., 2000. Dynamics and size structure of phytoplankton in the coastal waters of Singapore. J. Plankton Res. 22, 1465-1484.

Green, S.A., Blough, N.V., 1994. Optical absorption and fluorescence properties of chromophoric dissolved organic matter in natural waters. Limnol. Oceanogr. 39, 1903-1916.

Guest, J.R., Tun, K., Low, J., Vergés, A., Marzinelli, E.M., Campbell, A.H., Bauman, A.G., Feary, D.A., Chou, L.M., Steinberg, P.D., 2016. 27 years of benthic and coral community dynamics on turbid, highly urbanised reefs off Singapore. Sci. Rep. 6, 36260.

Hansen, H.P., Koroleff, F., 1999. Determination of nutrients. Methods of Seawater Analysis, 159-228.

Heery, E.C., Hoeksema, B.W., Browne, N.K., Reimer, J.D., Ang, P.O., Huang, D., Friess, D.A., Chou, L.M., Loke, L.H.L., Saksena-Taylor, P., Alsagoff, N., Yeemin, T., Sutthacheep, M., Vo, S.T., Bos, A.R., Gumanao, G.S., Syed Hussein, M.A., Waheed, Z., Lane, D.J.W., Johan, O., Kunzmann, A., Jompa, J., Suharsono, Taira, D., Bauman, A.G., Todd, P.A., 2018. Urban coral reefs: Degradation and resilience of hard coral assemblages in coastal cities of East and Southeast Asia. Mar. Pollut. Bull. 135, 654-681.

Huang, D., Tun, K.P.P., Chou, L.M., Todd, P.A., 2009. An inventory of zooxanthellate scleractinian corals in Singapore, including 33 new records. Raffles Bull. Zool. 22, 69-80.

Huang, T.H., Chen, C.T.A., Tseng, H.C., Lou, J.Y., Wang, S.L., Yang, L., Kandasamy, S., Gao, X., Wang, J.T., Aldrian, E., Jacinto, G.S., Anshari, G.Z., Sompongchaiyakul, P., Wang, B.J., 2017. Riverine carbon fluxes to the South China Sea. J. Geophys. Res. Biogeosci. 122, 1239-1259.

Januchowski-Hartley, F.A., Bauman, A.G., Morgan, K.M., Seah, J.C.L., Huang, D., Todd, P.A., 2020. Accreting coral reefs in a highly urbanized environment. Coral Reefs 39, 717-731.

Jennerjahn, T.C., 2012. Biogeochemical response of tropical coastal systems to present and past environmental change. Earth-Sci. Rev. 114, 19-41.

Jennerjahn, T.C., Ittekkot, V., Klöpper, S., Adi, S., Purwo Nugroho, S., Sudiana, N., Yusmal, A., Prihartanto, Gaye-Haake, B., 2004. Biogeochemistry of a tropical river affected by human activities in its catchment: Brantas River estuary and coastal waters of Madura Strait, Java, Indonesia. Estuar. Coast. Shelf Sci. 60, 503-514.

Jennerjahn, T.C., Knoppers, B.A., Souza, W.F.L., Brunskill, G.J., Silva, E.I.L., 2006. Factors controlling dissolved silica in tropical rivers, in: Ittekkot, V., Unger, D., Humborg, C., Tac An, N. (Eds.), The Silicon Cycle: Human Perturbations and Impacts on Aquatic Systems. Island Press, pp. 29-51.

Jiang, S., Müller, M., Jin, J., Wu, Y., Zhu, K., Zhang, G., Mujahid, A., Rixen, T., Muhamad, M.F., Sia, E.S.A., Jang, F.H.A., Zhang, J., 2019. Dissolved inorganic nitrogen in a tropical estuary in Malaysia: transport and transformation. Biogeosciences 16, 2821-2836.

Kartadikaria, A.R., Watanabe, A., Nadaoka, K., Adi, N.S., Prayitno, H.B., Soemorumekso, S., Muchtar, M., Triyulianti, I., Setiawan, A., Suratno, S., Khasanah, E.N., 2015. CO_2 sink/source characteristics in the tropical Indonesian seas. J. Geophys. Res. Oceans 120, 7842-7856.

Ke, Z., Tan, Y., Ma, Y., Huang, L., Wang, S., 2014. Effects of surface current patterns on spatial variations of phytoplankton community and environmental factors in Sunda shelf. Cont. Shelf Res. 82, 119-127.

Kendall, C., Elliott, E.M., Wankel, S.D., 2007. Tracing Anthropogenic Inputs of Nitrogen to Ecosystems. Stable Isotopes in Ecology and Environmental Science, 375-449.

Kérouel, R., Aminot, A., 1997. Fluorometric determination of ammonia in sea and estuarine waters by direct segmented flow analysis. Mar. Chem. 57, 265-275.

Kuwahara, V.S., Nakajima, R., Othman, B.H.R., Kushairi, M.R.M., Toda, T., 2010. Spatial variability of UVR attenuation and bio-optical factors in shallow coral-reef waters of Malaysia. Coral Reefs 29, 693-704.

Lee, T., Fournier, S., Gordon, A.L., Sprintall, J., 2019. Maritime Continent water cycle regulates low-latitude chokepoint of global ocean circulation. Nat. Commun. 10, 2103.

Li, C., Li, S.-L., Yue, F.-J., He, S.-N., Shi, Z.-B., Di, C.-L., Liu, C.-Q., 2020. Nitrate sources and formation of rainwater constrained by dual isotopes in Southeast Asia: Example from Singapore. Chemosphere 241, 125024.

Lim, J.H., Lee, C.W., Bong, C.W., 2021. Investigating factors driving phytoplankton growth and grazing loss rates in waters around Peninsular Malaysia. Journal of Oceanology and Limnology 39, 148-159.

Lim, J.H., Lee, C.W., Bong, C.W., Affendi, Y.A., Hii, Y.S., Kudo, I., 2018. Distributions of particulate and dissolved phosphorus in aquatic habitats of Peninsular Malaysia. Mar. Pollut. Bull. 128, 415-427.

Lim, J.H., Lee, C.W., Kudo, I., 2015. Temporal variation of phytoplankton growth and grazing loss in the west coast of Peninsular Malaysia. Environ. Monit. Assess. 187, 246.

Liu, H., Wu, C., Xu, W., Wang, X., Thangaraj, S., Zhang, G., Zhang, X., Zhao, Y., Sun, J., 2020. Surface Phytoplankton Assemblages and Controlling Factors in the Strait of Malacca and Sunda Shelf. Front. Mar. Sci. 7, 33.

Lønborg, C., Álvarez–Salgado, X.A., Duggan, S., Carreira, C., 2018. Organic matter bioavailability in tropical coastal waters: The Great Barrier Reef. Limnol. Oceanogr. 63, 1015-1035.

Lønborg, C., McKinna, L.I.W., Slivkoff, M.M., Carreira, C., 2021a. Coloured dissolved organic matter dynamics in the Great Barrier Reef. Cont. Shelf Res. 219, 104395.

Lønborg, C., Müller, M., Butler, E.C.V., Jiang, S., Ooi, S.K., Trinh, D.H., Wong, P.Y., Ali, S.M., Cui, C., Siong, W.B., Yando, E.S., Friess, D.A., Rosentreter, J.A., Eyre, B.D., Martin, P., 2021b. Nutrient cycling in tropical and temperate coastal waters: Is latitude making a difference? Estuar. Coast. Shelf Sci. 262, 107571.

Lueker, T.J., Dickson, A.G., Keeling, C.D., 2000. Ocean pCO_2 calculated from dissolved inorganic carbon, alkalinity, and equations for K_1 and K_2: validation based on laboratory measurements of CO_2 in gas and seawater at equilibrium. Mar. Chem. 70, 105-119.

Ma, J., Yuan, Y., Zhou, T., Yuan, D., 2017. Determination of total phosphorus in natural waters with a simple neutral digestion method using sodium persulfate. Limnol. Oceanogr. Methods 15, 372-380.

Martin, P., Cherukuru, N., Tan, A.S.Y., Sanwlani, N., Mujahid, A., Müller, M., 2018. Distribution and cycling of terrigenous dissolved organic carbon in peatland-draining rivers and coastal waters of Sarawak, Borneo. Biogeosciences 15, 6847-6865.

Martin, P., Sanwlani, N., Lee, T.W.Q., Wong, J.M.C., Chang, K.Y.W., Wong, E.W.S., Liew, S.C., 2021. Dissolved organic matter from tropical peatlands reduces shelf sea light availability in the Singapore Strait, Southeast Asia. Mar. Ecol. Prog. Ser. 672, 89-109.

948 Mayorga, E., Seitzinger, S.P., Harrison, J.A., Dumont, E., Beusen, A.H.W., Bouwman, A.F.,
949 Fekete, B.M., Kroeze, C., Van Drecht, G., 2010. Global Nutrient Export from
950 WaterSheds 2 (NEWS 2): Model development and implementation. Environ. Model.
951 Software 25, 837-853.
952 Mishra, S., Page, S.E., Cobb, A.R., Lee, J.S.H., Jovani-Sancho, A.J., Sjögersten, S., Jaya, A.,
953 Aswandi, Wardle, D.A., 2021. Degradation of Southeast Asian tropical peatlands and
954 integrated strategies for their better management and restoration. J. Appl. Ecol. 58,
955 1370-1387.
956 Mizubayashi, K., Kuwahara, V.S., Segaran, T.C., Zaleha, K., Effendy, A.W.M., Kushairi,
957 M.R.M., Toda, T., 2013. Monsoon variability of ultraviolet radiation (UVR) attenuation
958 and bio-optical factors in the Asian tropical coral-reef waters. Estuar. Coast. Shelf Sci.
959 126, 34-43.
960 Moore, S., Evans, C.D., Page, S.E., Garnett, M.H., Jones, T.G., Freeman, C., Hooijer, A.,
961 Wiltshire, A.J., Limin, S.H., Gauci, V., 2013. Deep instability of deforested tropical
962 peatlands revealed by fluvial organic carbon fluxes. Nature 493, 660-663.
963 Morgan, K.M., Moynihan, M.A., Sanwlani, N., Switzer, A.D., 2020. Light Limitation and
964 Depth-Variable Sedimentation Drives Vertical Reef Compression on Turbid Coral
965 Reefs. Front. Mar. Sci. 7, 931.
966 Moynihan, M.A., Goodkin, N.F., Morgan, K.M., Kho, P.Y.Y., Lopes dos Santos, A., Lauro,
967 F.M., Baker, D.M., Martin, P., 2021. Coral-associated nitrogen fixation rates and
968 diazotrophic diversity on a nutrient-replete equatorial reef. The ISME Journal.
969 Nichols, R.S., Martin, P., 2021. Low biodegradability of dissolved organic matter from
970 Southeast Asian peat-draining rivers. J. Geophys. Res. Biogeosci. 126,
971 e2020JG006182.
972 Ning, X., Chai, F., Xue, H., Cai, Y., Liu, C., Shi, J., 2004. Physical-biological oceanographic
973 coupling influencing phytoplankton and primary production in the South China Sea. J.
974 Geophys. Res. Oceans 109, C10005.
975 Nittrouer, C.A., Brunskill, G.J., Figueiredo, A.G., 1995. Importance of tropical coastal
976 environments. Geo-Mar. Lett. 15, 121-126.
977 Pacella, S.R., Brown, C.A., Waldbusser, G.G., Labiosa, R.G., Hales, B., 2018. Seagrass
978 habitat metabolism increases short-term extremes and long-term offset of CO_2 under
979 future ocean acidification. Proc. Natl. Acad. Sci. 115, 3870.
980 Page, H.N., Courtney, T.A., De Carlo, E.H., Howins, N.M., Koester, I., Andersson, A.J.,
981 2019. Spatiotemporal variability in seawater carbon chemistry for a coral reef flat in
982 Kāneʻohe Bay, Hawaiʻi. Limnol. Oceanogr. 64, 913-934.
983 Partelow, S., Schlüter, A., von Wehrden, H., Jänig, M., Senff, P., 2018. A Sustainability
984 Agenda for Tropical Marine Science. Conservation Letters 11, e12351.
985 Perez, F.F., Fraga, F., 1987. Association constant of fluoride and hydrogen ions in seawater.
986 Mar. Chem. 21, 161-168.
987 Ren, H., Sigman, D.M., Martínez-García, A., Anderson, R.F., Chen, M.-T., Ravelo, A.C.,
988 Straub, M., Wong, G.T.F., Haug, G.H., 2017. Impact of glacial/interglacial sea level
989 change on the ocean nitrogen cycle. Proc. Natl. Acad. Sci. 114, E6759.
990 Schaefer, S.C., Hollibaugh, J.T., 2017. Temperature Decouples Ammonium and Nitrite
991 Oxidation in Coastal Waters. Environ. Sci. Technol. 51, 3157-3164.
992 Siegel, H., Gerth, M., Stottmeister, I., Baum, A., Samiaji, J., 2019. Remote Sensing of
993 Coastal Discharge of SE Sumatra (Indonesia), in: Barale, V., Gade, M. (Eds.), Remote
994 Sensing of the Asian Seas. Springer International Publishing, Cham, pp. 359-376.
995 Sigman, D.M., Casciotti, K.L., Andreani, M., Barford, C., Galanter, M., Böhlke, J.K., 2001.
996 A Bacterial Method for the Nitrogen Isotopic Analysis of Nitrate in Seawater and
997 Freshwater. Anal. Chem. 73, 4145-4153.

998 Sinha, E., Michalak, A.M., Calvin, K.V., Lawrence, P.J., 2019. Societal decisions about
999 climate mitigation will have dramatic impacts on eutrophication in the 21st century.
1000 Nat. Commun. 10, 939.
1001 Stoltenberg, L., Schulz, K.G., Lantz, C.A., Cyronak, T., Eyre, B.D., 2021. Late Afternoon
1002 Seasonal Transition to Dissolution in a Coral Reef: An Early Warning of a Net
1003 Dissolving Ecosystem? Geophys. Res. Lett. 48, e2020GL090811.
1004 Sundarambal, P., Tkalich, P., Balasubramanian, R., 2010. Impact of biomass burning on
1005 ocean water quality in Southeast Asia through atmospheric deposition: eutrophication
1006 modeling. Atmos. Chem. Phys. 10, 11337-11357.
1007 Susanto, R.D., Zexun, W., Adi, T.R., Guohong, F., Bin, F., Agus, S., Teguh, A., Shujiang, L.,
1008 Mukti, T., Agus, S., 2016. Oceanography Surrounding Krakatau Volcano in the Sunda
1009 Strait, Indonesia. Oceanography 29, 264-272.
1010 Tan, A., 2020. As some fish farms in Johor Strait near maximum production levels,
1011 authorities eye southern expansion, The Straits Times, Singapore.
1012 Tanzil, J.T.I., Goodkin, N.F., Sin, T.M., Chen, M.L., Fabbro, G.N., Boyle, E.A., Lee, A.C.,
1013 Toh, K.B., 2019. Multi-colony coral skeletal Ba/Ca from Singapore's turbid urban
1014 reefs: Relationship with contemporaneous in-situ seawater parameters. Geochim.
1015 Cosmochim. Acta 250, 191-208.
1016 Team, R.C., 2020. R: A language and environment for statistical computing. R Foundation
1017 for Statistical Computing, Vienna, Austria.
1018 Todd, P.A., Heery, E.C., Loke, L.H.L., Thurstan, R.H., Kotze, D.J., Swan, C., 2019. Towards
1019 an urban marine ecology: characterizing the drivers, patterns and processes of marine
1020 ecosystems in coastal cities. Oikos 128, 1215-1242.
1021 Tomascik, T., Suharsono, Mah, A., 1994. Case histories: a historical perspective of the
1022 natural and anthropogenic impacts in the Indonesian Archipelago with a focus on the
1023 Kepulauan Seribu, Java Sea. Colloquium on Global Aspects of Coral Reefs: Health,
1024 Hazard and History.
1025 Troxler, T.G., 2007. Patterns of phosphorus, nitrogen and $\delta^{15}N$ along a peat development
1026 gradient in a coastal mire, Panama. J. Trop. Ecol. 23, 683-691.
1027 Uppström, L.R., 1974. The boron/chlorinity ratio of deep-sea water from the Pacific Ocean.
1028 Deep Sea Research and Oceanographic Abstracts 21, 161-162.
1029 Veron, J.E.N., Devantier, L.M., Turak, E., Green, A.L., Kininmonth, S., Stafford-Smith, M.,
1030 Peterson, N., 2009. Delineating the Coral Triangle. Galaxea 11, 91-100.
1031 Verwega, M.T., Somes, C.J., Schartau, M., Tuerena, R.E., Lorrain, A., Oschlies, A., Slawig,
1032 T., 2021. Description of a global marine particulate organic carbon-13 isotope data set.
1033 Earth Syst. Sci. Data 13, 4861-4880.
1034 Vieillard, A.M., Newell, S.E., Thrush, S.F., 2020. Recovering From Bias: A Call for Further
1035 Study of Underrepresented Tropical and Low-Nutrient Estuaries. J. Geophys. Res.
1036 Biogeosci. 125, e2020JG005766.
1037 Welschmeyer, N.A., 1994. Fluorometric analysis of chlorophyll *a* in the presence of
1038 chlorophyll *b* and pheopigments. Limnol. Oceanogr. 39, 1985-1992.
1039 Wit, F., Rixen, T., Baum, A., Pranowo, W.S., Hutahaean, A.A., 2018. The Invisible Carbon
1040 Footprint as a hidden impact of peatland degradation inducing marine carbonate
1041 dissolution in Sumatra, Indonesia. Sci. Rep. 8, 17403.
1042 Zhang, R., Wang, X.T., Ren, H., Huang, J., Chen, M., Sigman, D.M., 2020. Dissolved
1043 Organic Nitrogen Cycling in the South China Sea From an Isotopic Perspective. Glob.
1044 Biogeochem. Cycles 34, e2020GB006551.
1045 Zhou, Y., Evans, C.D., Chen, Y., Chang, K.Y.W., Martin, P., 2021. Extensive
1046 Remineralization of Peatland-Derived Dissolved Organic Carbon and Ocean

1047 Acidification in the Sunda Shelf Sea, Southeast Asia. J. Geophys. Res. Oceans 126,
1048 e2021JC017292.
1049 Zhou, Y., Martin, P., Müller, M., 2019. Composition and cycling of dissolved organic matter
1050 from tropical peatlands of coastal Sarawak, Borneo, revealed by fluorescence
1051 spectroscopy and parallel factor analysis. Biogeosciences 16, 2733-2749.
1052

Supplementary Material

P. Martin *et al.* Monsoon-driven biogeochemical dynamics in an equatorial shelf sea: time-series observations in the Singapore Strait

Table S1. Relationships between biogeochemical parameters and CDOM a_{350}. Slope and intercept estimates are given together with their respective standard errors; non-significant intercepts are marked "NS". P-values refer to the regression slopes.

Parameter	Slope estimate (SE)	Intercept estimate (SE)	Statistics
NO_3^-	1.79 (0.13)	-0.05 (0.10), NS	r^2=0.612, p<0.0001
PO_4^{3-}	0.118 (0.008)	0.048 (0.007)	r^2=0.611, p<0.0001
$Si(OH)_4$	4.20 (0.33)	2.98 (0.26)	r^2=0.563, p<0.0001
NO_2^-	0.234 (0.044)	0.010 (0.035)	r^2=0.186, p<0.0001
DOC	14.3 (1.18)	68.6 (0.95)	r^2=0.540, p<0.0001
DOP	-0.097 (0.015)	0.160 (0.013)	r^2=0.311, p<0.0001
δ^{13}C-POC	-1.24 (0.31)	-20.2 (0.23)	r^2=0.143, p<0.0001
δ^{15}N-PN	-0.907 (0.241)	5.01 (0.19)	r^2=0.116, p<0.001
$\delta^{15}N\text{-}NO_x^-$	2.59 (0.96)	4.42 (0.75)	r^2=0.376, p<0.05

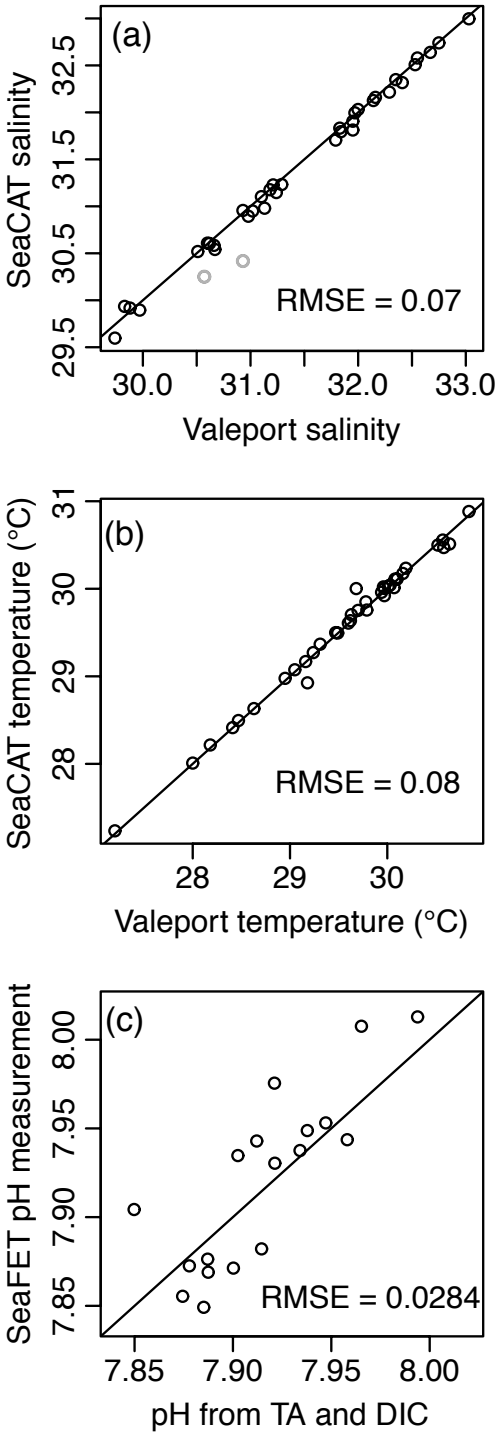

Fig. S1. Comparison of (a) salinity and (b) temperature measured by Seabird SeaCAT moored CTD at Kusu and by Valeport FastCTD profiler at Kusu. The RMSE in (a) excludes the two outliers indicated in grey. (c) Comparison of seawater pH measured by SeaFET pH sensor at Kusu and pH calculated from laboratory measurements of total alkalinity and dissolved inorganic carbon concentration. Solid lines show 1:1 relationships.

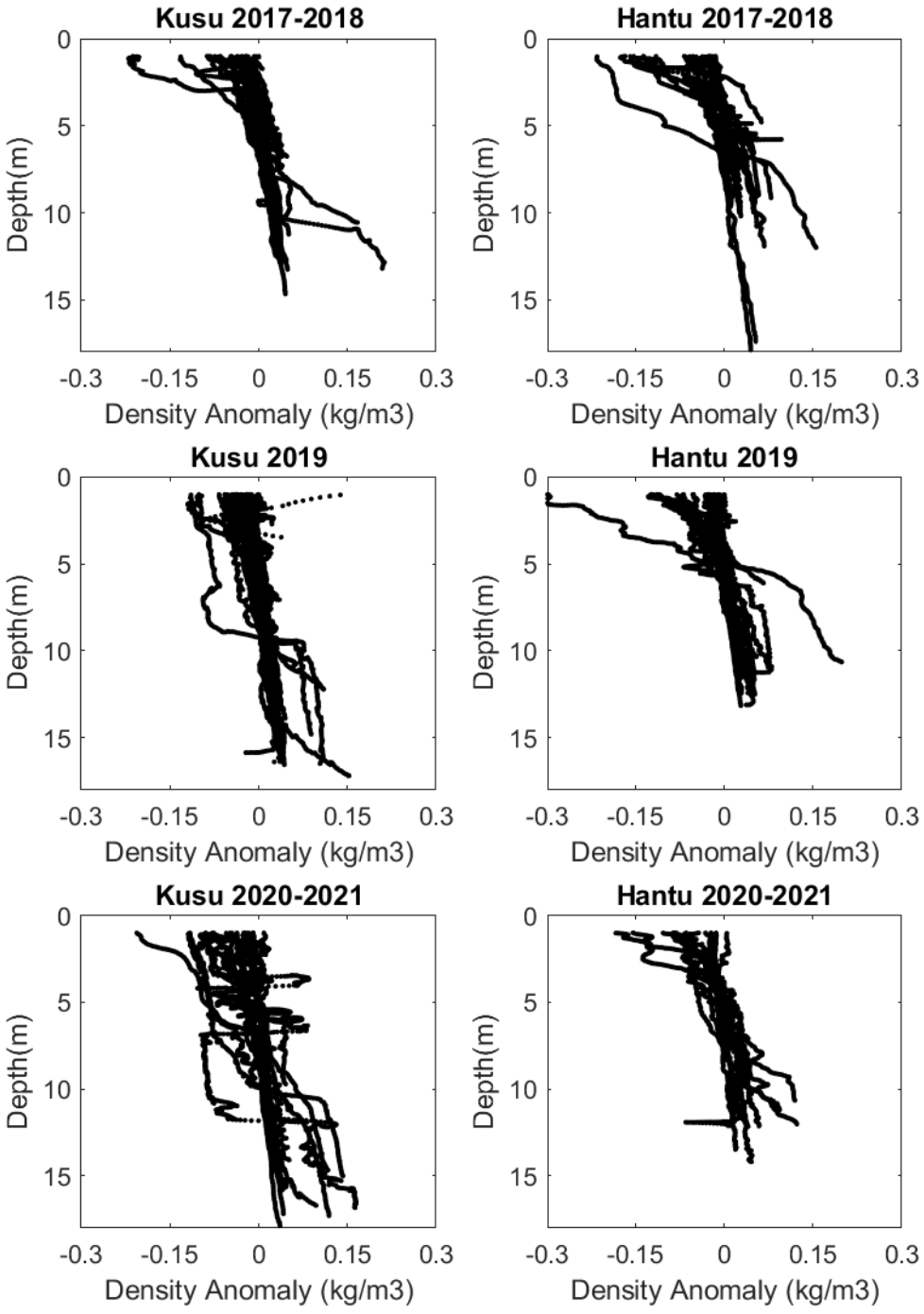

Fig. S2. Vertical profiles of potential density anomaly calculated from Valeport FastCTD profile data (calculated by subtracting the mean potential density of each profile). Note that there is typically no clear pycnocline, indicating little consistent water column stratification.

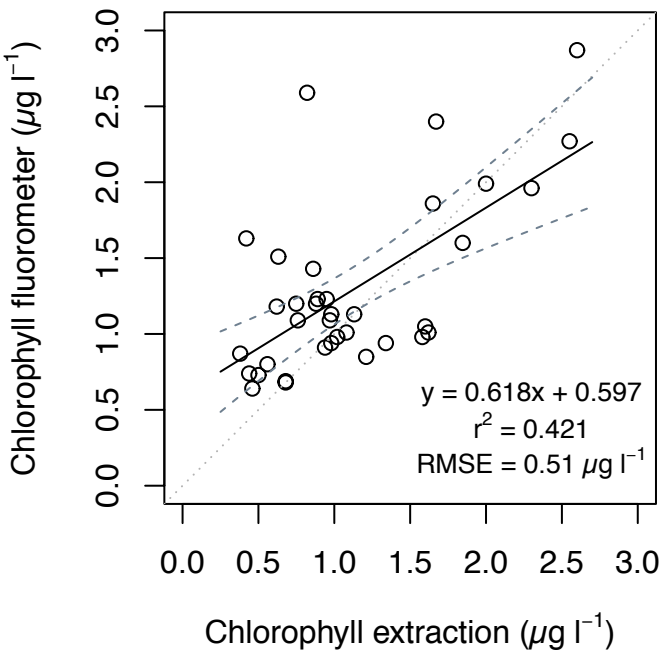

Fig. S3. Comparison of chlorophyll-*a* as measured *in-vivo* by the fluorometer on the Valeport FastCTD *versus* measurements from filtered water samples that were extracted in acetone and measured in the laboratory. Solid black and dashed dark grey lines indicate linear regression and 95% confidence interval. Dotted grey line in the 1:1 relationship.

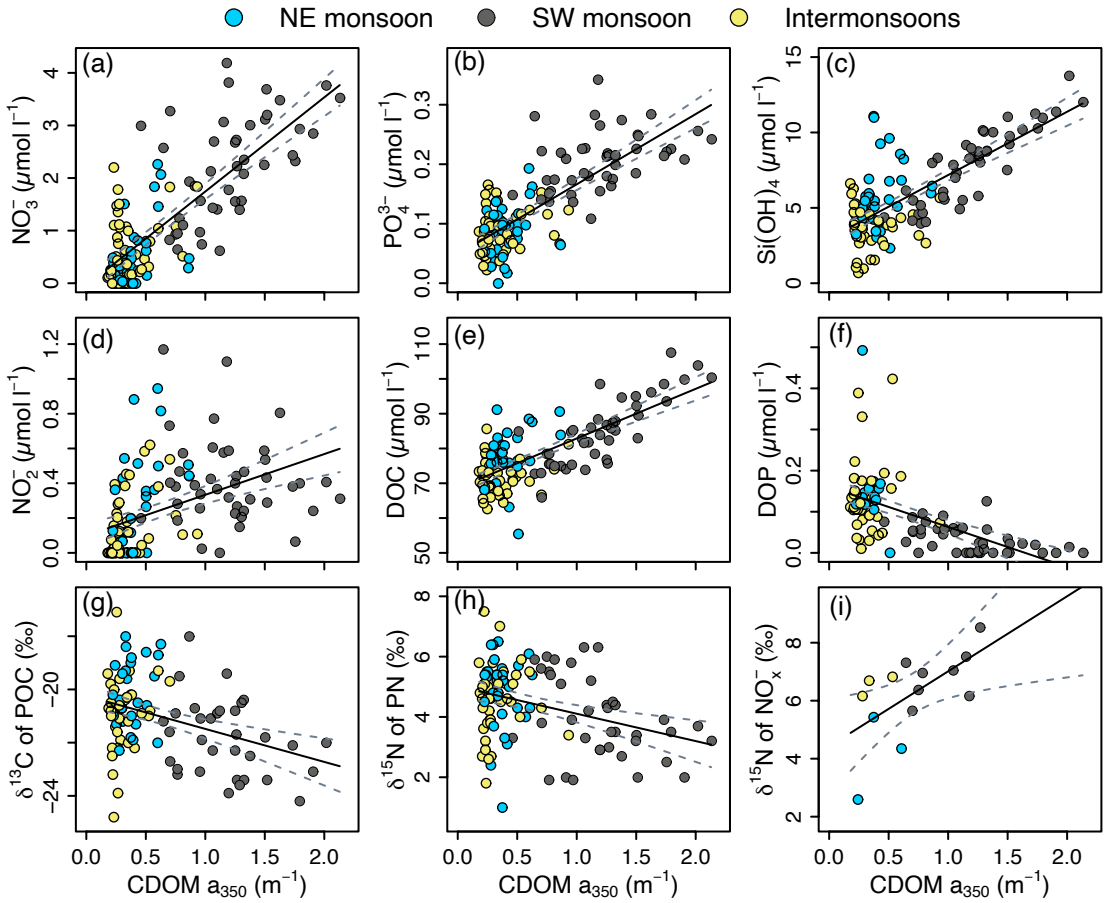

Fig. S4. Relationships between parameters that showed significant relationships to salinity and coloured dissolved organic matter (measured as absorption coefficient at 350 nm; a_{350}). Solid black and dashed dark grey lines indicate linear regressions and 95% confidence intervals.